TOUCH-SPINNING OF MANUKA HONEY-INCORPORATED TISSUE-ENGINEERING VASCULAR GRAFTS REDUCES HOST-BIOMATERIAL ACUTE INFLAMMATION *IN VITRO*

Evan N. Main, Alexandra E. Snyder, Audrey N. Alberson, Jada K. Sandridge, Adeline E. Nordmoe, Gary L. Bowlin*

Department of Biomedical Engineering, University of Memphis, 3796 Norriswood Ave, 38152 Memphis, TN, USA

* Correspondence: glbowlin@memphis.edu (Gary L. Bowlin)

Abstract

Neutrophils utilize a specialized form of cell death, Neutrophil Extracellular Traps (NETs), to kill and trap invading pathogens; however, dysregulated NET release (NETosis) can drive tissue damage and fibrosis at host–biomaterial interfaces. Manuka honey exhibits potent antibacterial and emerging anti-inflammatory properties within and outside electrospun vascular tissue-engineering templates. Because current small-diameter vascular graft materials do not adequately resolve neutrophil-driven acute inflammation, they often fail, and no synthetic grafts below 4 mm in diameter are currently approved for clinical use, leaving a substantial unmet need in cardiovascular medicine. This investigation tested two central hypotheses: (1) incorporating Manuka honey into polydioxanone (PDO) touch-spun vascular templates would reduce NET formation, and (2) the touch-spinning method, which uses mechanical rather than electrical forces to draw fibers, would preserve Manuka honey's bioactivity more effectively than traditional biomaterial fabrication approaches. Templates were fabricated from 185 mg/mL polydioxanone (PDO) containing 0%, 0.1%, 1%, or 10% Manuka honey and co-cultured with primary human neutrophils for 4 hours. NETosis was quantified from culture supernatants using a myeloperoxidase (MPO) assay. Mechanical properties were evaluated following ANSI/AAMI standards for vascular graft prostheses and compared across Manuka concentrations relative to 0% controls and native blood vessels. Findings from this study demonstrate that Manuka honey can be integrated into touch-spun vascular templates without compromising the required mechanical properties. Moreover, Manuka-incorporated templates retained Manuka honey's neutrophil-modulating effects more effectively than electrospun counterparts. Finally, the sustained release profile of Manuka honey from these grafts aligns well with the acute, neutrophil-dominant inflammatory window following biomaterial implantation.

Keywords: *NETosis, neutrophil, vascular tissue engineering, touch-spinning, host-biomaterial response, biomaterials*

[Engineering of Biomaterials 174 (2026) 05]

doi:10.34821/eng.biomat.174.2026.05

Submitted: 2026-01-11, Accepted: 2026-03-03, Published: 2026-03-10

Introduction

On a global scale, cardiovascular disease is the number one cause of death and is expected to increase in prevalence for the foreseeable future [1]. Predictions suggest cardiovascular disease-related mortalities will rise to 23.3 million cases annually by 2030. Commonly, these related mortalities present as coronary heart disease, deep vein thrombosis, peripheral arterial disease, and cerebrovascular disease [2]. Treatments for cardiovascular disease typically fall into three categories: first, preventative lifestyle changes (such as diet and exercise), and pharmaceutical interventions. Secondly, endovascular surgical procedures (angioplasty, stent insertion, atherectomy) are used to restore blood flow by dilating the blood vessel or removing the blockage. Lastly, should the two prior options fail, the occluded or damaged blood vessels are excised and replaced or bypassed using a vascular graft. Currently, vascular bypass grafting is considered the gold standard for long-term (with a life expectancy of greater than two years) revascularization therapies, with approximately 400,000 coronary artery bypass grafting surgeries performed in America alone [3-5]. The preferred materials for vascular grafts are autologous arteries or veins, specifically the saphenous vein (SV), which is most commonly used despite a reported failure rate of around 50% after 10 years following coronary artery bypass grafting (CABG) or femoropopliteal bypass (Fem-pop) surgeries [6]. An additional limitation to autologous grafts is the poor quality of the vein due to the pathology of cardiovascular disease or comorbidities, limited availability, and donor site morbidity. Synthetic materials such as the synthetic vascular graft gold standard of expanded polytetrafluoroethylene (ePTFE) have shown acceptable mechanical properties and patency (the ability of the vessel to remain unobstructed) in large diameter applications such as aortoiliac bypasses (where the diameter of the vessel is above 8 mm) or in mid-diameter arteries such as the femoral or carotid (with diameters ranging between 6 mm and 8 mm) [7, 8]. However, for blood vessels smaller than 6 mm, the efficacy of synthetic grafts significantly decreases. This steep decline in viability primarily results from poor graft patency (FIG. 1), which is caused by occlusions due to hyperplasia, thrombosis, infection, or atherosclerosis [4].

A primary underlying cause of the reduced efficacy of small-diameter vascular grafts is the host response to implanted biomaterials. For example, the host response to ePTFE is similar to that of a splinter. The body never recognizes the implant as its own and thus isolates it from the body after a continued immune attack. The initial inflammatory response, dominated by neutrophils, creates a microenvironment that is conducive to sustained immune cell recruitment and signaling. The constant influx of pro-inflammatory-primed immune cells leads to ongoing oxidative and enzymatic damage to the biomaterial and surrounding tissue [9]. In many such cases, weeks after implantation, the device is encapsulated by a dense, disorganized fibrous collagen network [10]. This sustained immune attack, resulting from the failure to resolve the initial acute phase of inflammation, leads to impaired revascularization, scar tissue deposition, and ultimately device failure (FIG. 2). By avoiding excessive acute inflammation, the implant microenvironment can be shifted away from fibrous encapsulation toward revascularization and reintegration with the host vasculature.

These effects are even more deleterious in small-diameter vascular grafts for the following reasons. The end-stage fibrotic capsule has been shown to be non-uniformly constrictive, causing flow disturbances within the vessel and thereby increasing the risk of thrombosis. The capsule is also nonelastic, causing a discrepancy between the mechanical properties of the vasculature and the device, potentially

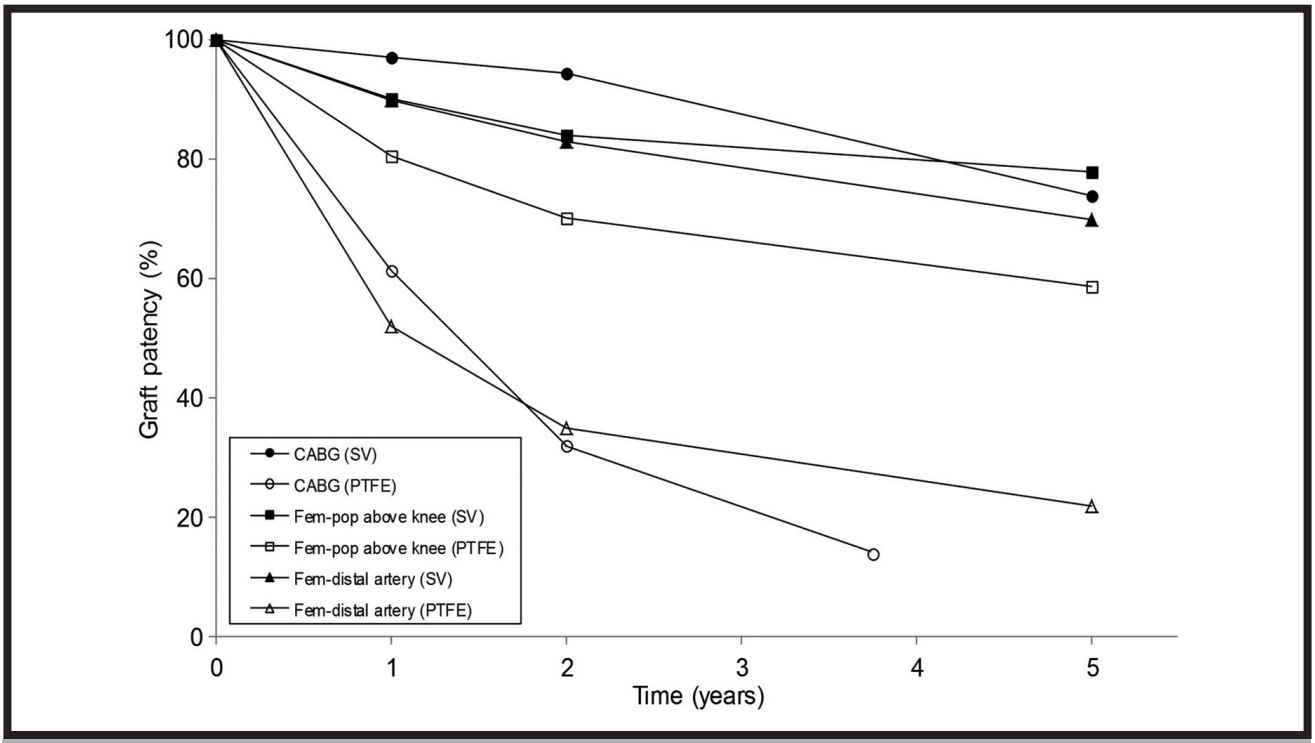

FIG. 1. Poor patency rates in small-diameter applications of synthetic vascular grafts. Reprinted with permission from Pashneh-Tala, S., S. MacNeil, and F. Claeyssens, 2016. Copyright Mary Ann Liebert [4].

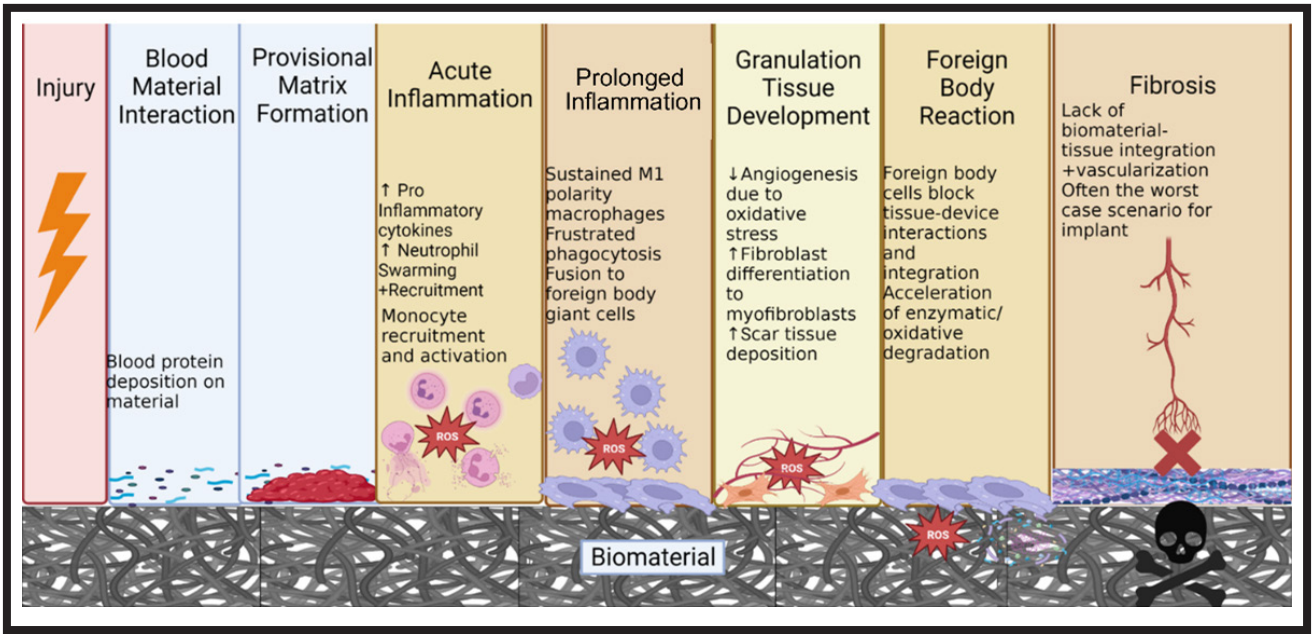

FIG. 2. Poor resolution of inflammation leads to fibrous encapsulation and failure of the implant. Created with Biorender (2025).

causing hyperplasic cell proliferation [11]. Additionally, the avascularity of the device due to the fibrous capsule will prevent complete healing and reendothelialization of the vessel [12]. Finally, sustained oxidative and enzymatic degradation by neutrophils and macrophages, driven by unresolved inflammation, can directly lead to device failure and rupture. Small-diameter grafts are far more prone to failure from these mechanisms because even small occlusions, flow disturbances, or mechanical mismatches can significantly affect the total flow through such a small diameter.

Because of the limited ability of vascular grafts to resolve acute immunity and prevent the perpetuation of inflammation, there are currently no small-diameter synthetic vascular grafts approved by regulatory agencies for use in the clinic today [11]. The lack of synthetic vascular grafts with inner diameters below 4 mm available on the market leaves an enormous unmet need for the prevention of the approximately 1 million limbs amputated worldwide each year [4]. Additionally, synthetic small-diameter grafts could help alleviate the limitations of using autologous blood vessels in approximately 400,000 cardiac bypass surgeries performed in America each year.

The response of neutrophils to an implanted biomaterial can be categorized in three main ways. Neutrophils can act as potent signalers, releasing a multitude of pro-inflammatory cytokines and chemokines in response to foreign material. These signals recruit additional immune cells, including neutrophils, to the site of implantation, leading to a shift towards

pro-inflammatory phenotypes in macrophages and neutrophils that arrive there. Additionally, neutrophils can undergo a specialized form of cell death called NETosis, wherein they release neutrophil extracellular traps (NETs). These NETs consist of histones entangled within fibrillary, interlinked strands of chromatin, which are coated with proteins derived from neutrophil granules and act to sequester and degrade foreign materials. During an overabundant neutrophil response to an implanted biomaterial, NETs wall off the biomaterial's surface and block proper tissue integration. During NETosis, pro-inflammatory signals and degradative enzymes are also released. Neutrophils are also potent generators of ROS, using oxidative stress to damage and degrade foreign materials [13, 14]. The signaling, NET-forming, and ROS-generating capacities of neutrophils make them highly effective at defending the body from invading pathogens. In the case of biomaterial implantation, however, where the foreign body is not a threat to be eliminated, excessive neutrophil activity can have drastic consequences for the implant microenvironment, extending acute inflammation to the point of pathology.

Neutrophil inflammatory behaviors are highly linked with intracellular ROS production. Heightened ROS levels within the cytoplasm of neutrophils activate inhibitory kinase kinase (IKK), activating the pro-inflammatory NF-κB pathway, increasing the transcription of pro-inflammatory cytokines, recruiting more neutrophils and other immune cells to the implant area [15]. Antioxidant therapeutics have been demonstrated to reduce the activation of NF-κB and thus reduce the expression of key inflammatory signals in neutrophils [16]. Similarly, intracellular ROS production is crucial in releasing neutrophil elastase (NE) and myeloperoxidase (MPO) from neutrophil granules during NETosis [17]. Cytoskeletal reorganization during NETosis is highly dependent on MPO-initiated neutrophil NE release. Methyl syringate, the primary phenolic fraction of Manuka honey, has shown promise in inhibiting MPO and has demonstrated a strong inhibitory effect on both NETosis and intracellular ROS activity from stimulated neutrophils [13, 18, 19]. However, the ability of methyl syringate to be electrospun or incorporated into biomaterials has yet to be explored, nor has its ability to prevent infection. Thus, further exploration of methyl syringate as a biomaterial additive is underway. As such, this paper focused on enhancing the known capacity of Manuka honey to yield beneficial effects as a biomaterial additive while circumventing the current limitations imposed by traditional biomaterial fabrication techniques.

Previous research has shown that Manuka honey reduces neutrophil superoxide production, chemotaxis, and NF-κB activation within a therapeutic window of 0.5%-5% v/v [20]. While other reports demonstrate inhibition of NETosis and intracellular ROS activity. Investigations involving HL60 models have shown a dose-dependent decrease in ROS generation and IκBα (a pro-inflammatory cytokine release upstream signaling molecule) in response to co-culture with Manuka honey, with chemotaxis returning to control levels even at low honey concentrations, even in the presence of chemotactic peptide (fMLP) stimulation. Additionally, specific pro-inflammatory cytokine release profiles and degradative enzyme levels were decreased in response to Manuka honey. Manuka honey decreased dHL60 secretion of IL-1β, RANTES, MIP-1α, and ECM-degrading enzymes MMP-1 and MMP-9 [21-23]. Additionally, Manuka honey was incorporated into TES PDO templates at concentrations of 0.1, 1, or 10% v/v. This study found that when incorporated into the PDO template, Manuka honey reduced NET formation by up to 75%. However, 10% Manuka honey increased NET formation. Interestingly, this increase in NETosis at the 10% limit has not been observed in the absence of a PDO template, in which Manuka honey was co-cultured with phorbol-12-myristate-13-acetate (PMA) – stimulated neutrophils and reduced NETosis considerably [19, 24, 25]. A fundamental limitation of this study was the use of traditional electrospinning methods that employ high voltages of 14-25 kV, which could potentially damage the structure of the bioactive components in Manuka honey, thereby rendering it less effective at preventing neutrophil inflammatory behavior. Although the effects of electric fields on the bioactivity of anti-inflammatory and antioxidant compounds have not been investigated specifically in electrospinning and biomaterial fabrication, multiple studies have examined the effects of electric fields on phenols, flavonoids, and flavanols commonly found in foods during processing. These investigations have found that increasing both the voltage and the duration of voltage exposure decreased radical-scavenging activity, antioxidant capacity, flavonoids, and total phenolics [26-28]. Recent evidence has suggested that Manuka honey's ability to modulate inflammatory activity is directly tied to the primary phenolic component, methyl syringate, and potentially other flavonoid components, it stands to reason that the high voltages involved in electrospinning, electrospraying, as well as the long times that the material is subjected to voltage during fabrication, may have a detrimental effect on antioxidant efficacy.

Additionally, electrospinning may affect the incorporation of Manuka honey into the polymer, thereby influencing the template's release profile and mechanical properties. A 2015 study showed that honey incorporated into electrospun templates adversely affected mechanical properties. A later study showed that fiber melding occurred at higher honey concentrations in small-pore templates, suggesting that honey may alter fiber properties [24, 29]. The approach employed in this study to address these effects is the use of touch spinning, a method that creates fibrous polymer materials by applying mechanical force (via spinning glass rods) to drive the polymer solution to the target, thereby eliminating the need for high voltages (FIG. 3) [30-32]. This study aimed to leverage the promising findings of this fabrication technique to preserve the mechanical properties and release profiles of PDO templates, while reducing neutrophil inflammatory behaviors, as Manuka honey has demonstrated.

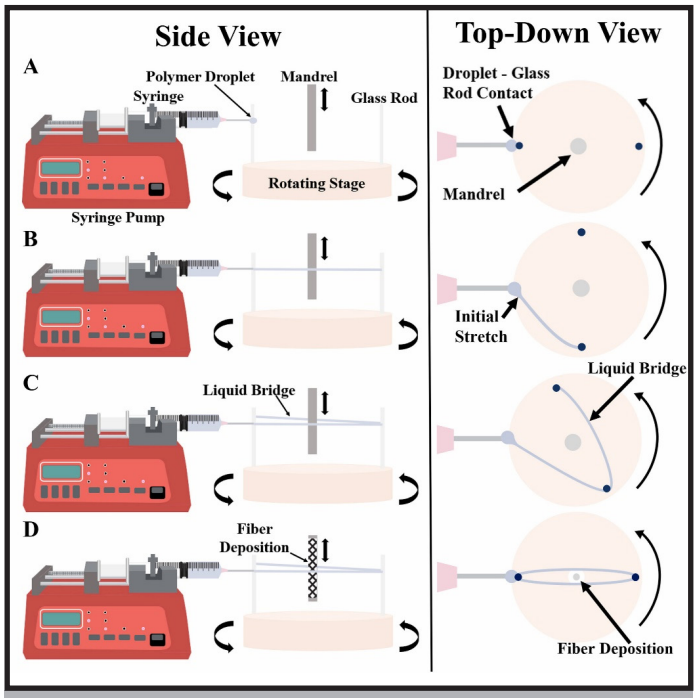

FIG. 3. Touch-Spinning to Avoid High Voltages While Allowing Fiber Angle Control in Biomaterial Fabrication. Adapted from Sandridge et. al. 2025 [32].

Recent advances in vascular tissue engineering using decellularized grafts have emphasized the importance of integrating bioactive components to enhance their efficacy. Decellularized extracellular matrices incorporating signaling peptides or with bioactive coatings designed to reduce thrombogenicity have demonstrated the capacity to promote favorable cellular responses [33-35]. These strategies, in parallel with advances in synthetic material development, have demonstrated the potential to improve graft integration and function within host tissues while mitigating acute inflammatory responses following implantation. Emerging approaches also explore alternative material sources and composite designs to address the limitations of conventional decellularized grafts. For example, therapeutics derived from plant-based materials have been shown to combine the structural benefits of decellularized matrices with enhanced biocompatibility, offering a promising pathway toward more mechanically viable vascular grafts [36]. In parallel, engineered composite allografts have gained attention for their capacity to reduce immunogenicity and prolonged acute inflammation through optimized decellularization and scaffold design [37].

Thus, this investigation aimed to test whether incorporating Manuka honey would affect the mechanical properties of PDO polymer scaffolds, potentially reducing their elasticity. Additionally, this study aimed to characterize the release profiles, examining any dependence on the initial Manuka honey concentration incorporated into the PDO polymer solution, as well as the timing of elution from the PDO template. These steps are vital for transitioning Manuka honey from an in vitro, standalone bioactive to a viable biomaterial additive. By selecting the most prevalent biodegradable material used in both the clinic and in polymer tissue engineering approaches, and determining the concentration of Manuka honey at which it is least susceptible to changes in mechanical properties due to incorporation, will further efforts in designing a singular and cohesive small-diameter vascular graft that can safely and effectively resolve acute inflammation [38-41]. Additionally, this study aimed to determine whether touch-spinning could produce a larger effect size in reducing NETosis compared to prior techniques, such as traditional electrospinning (TES), and whether the adverse effects observed at the upper limit of 10% Manuka honey in TES templates could be mitigated.

Materials and Methods

Synthetic graft fabrication

10 mL vials of Manuka honey were sonicated until fully liquefied. 0.5 mL of the honey was dispensed into a new 5 mL tube, and 4.5 mL of 1,1,1,3,3,3-hexafluoro-2-propanol (HFP, Oakwood Products, Inc., Estill, SC, USA) was added. The mixture was sonicated for 90 minutes. A serial dilution was performed from this 10% solution to create a 1% and 0.1% Manuka honey solution in HFP. As in previous literature, the control groups (0% Manuka honey) received 0.5 mL of deionized water to control for the percentage of missing HFP in the higher Manuka honey groups [29]. Polydioxanone (PDO, DIOXOMAXX®100, inherent viscosity 1.70 dL/g, Beswada Biomedical, Hillsborough, NJ, USA) was added to each solution at a concentration of 185 mg/mL and was allowed to dissolve overnight in Class B clear glass threaded vials (Fisherbrand™, Cat. No. 03-339-22D). Once dissolved, the solutions were placed into 3 mL syringes (Fisherbrand™, 14955457), and an 18-gauge 2-inch needle (McMaster-Carr, Elmhurst, IL, USA, Cat. No. 75165A249) was attached. The syringe was placed onto a NE-300 Just Infusion™ Syringe Pump (New Era Pump Systems, Inc., Farmingdale, NY, USA) set at a flow rate of 1.0 mL/hour. The fibers were touch-spun by setting the rotating stage (Figure 3) to 180 rpm (linear velocity: 0.90 m/s). To achieve an angle of 40°, the crank stepper motor (Figure 3) was set to 14 rpm (linear velocity: 0.05 m/s). The burst pressure samples were collected directly from a latex balloon covering the mandrel (Qualatex, Hamilton, ON, Canada, Cat. No. 43918). Eighteen samples of each concentration (10%, 1%, 0.1%, 0% Manuka honey) were collected and stored in a desiccator until mechanical testing, release studies, or neutrophil cell seeding.

Mechanical Characterization

One-half of the total templates (n = 48) were evaluated mechanically in both longitudinal and circumferential directions using a uniaxial testing frame (Test Resources, Shakopee, MN, USA) equipped with a 25 lbf load cell (Model SM-25-294, Test Resources). The thickness of each template was measured with a digital caliper (Model 547-516S, Mitutoyo, Kanagawa, Japan), and the width of each was measured with a ruler. The mechanical properties of the templates were evaluated for each Manuka honey concentration and compared with literature values for the native internal mammary artery and the saphenous vein [39, 42-44]. Additionally, Manuka honey incorporated templates were compared to templates that were not impregnated with Manuka honey to determine the sole effect of Manuka honey within the biomaterial.

Template morphology and fiber diameter were assessed via scanning electron microscopy (SEM). Sections of the templates were sputter-coated with a 5.0 nm coating of 60:40 gold-palladium in an argon atmosphere and visualized using SEM (Nova Nano 650 FEG, FEI Co., Hillsboro, OR, USA) with a field-emission gun operating at +20 kV, a spot size of 1.5, and a 5 mm working distance. Fiber diameters were analyzed using the General Image Fiber Tool in ImageJ (National Institutes of Health, Public Domain, BSD-2).

Longitudinal Uniaxial Elongation

The longitudinal tested templates (n=24) were cut into six 20 mm segments perpendicular to the longitudinal axis and soaked in Hank's Balanced Salt Solution (HBSS, Gibco™, Cat. No. 14025092) for 90 minutes in a CO2-free incubator at 37 degrees Celsius. The templates were placed into the grips of the testing frame with an initial separation distance of 8 mm, and the grips were separated at a rate of 50 mm/minute until failure. Data were recorded at a sampling rate of 50 samples per second. The ultimate tensile strength (UTS) was reported in megapascals (MPa) and calculated based on the initial cross-section of each template. The total percentage elongation was calculated and reported relative to the initial grip separation.

Circumferential Uniaxial Elongation

The circumferentially tested templates (n=24) were cut into 4 mm segments perpendicular to the longitudinal axis. Two 1.2 mm dowels were secured into a custom apparatus with an initial separation of 4 mm between the dowels. The segments were slid onto the two dowels, and the grips were separated at a rate of 50 mm/minute until failure. The data was recorded at a sampling rate of 50 samples per second. The UTS and Young's modulus were reported in MPa and calculated based on the initial cross-section of each template. The total percentage elongation was calculated and reported relative to the initial grip separation.

Suture Retention

The suture retention templates (n=24) were cut into 20 mm segments perpendicular to the longitudinal axis.

A single wall of each template was threaded with 5-0 REDILON™ monofilament (MYCO Medical Supplies, Inc., Cary, NC, USA) to form a half loop 2 mm below the template cut line. The bottom of the template was placed into the bottom vise grip, while the suture was fixed in the opposing vise grip with an initial grip separation of 13 mm. The grips were separated at a rate of 150 mm/min until failure, and data were recorded in grams-force at a sampling rate of 50 samples/s.

Burst Pressure

The templates utilized for burst pressure testing were fabricated directly onto a 160Q latex balloon (Qualatex, Wichita, KS, USA) by sliding the balloon directly over the mandrel. After completing fabrication, the balloon was stretched to separate the template from the balloon. The balloon and template were fixed onto a custom-designed burst pressure apparatus by placing the sample over barbed hose fittings. The sample was secured using 2-0 Black Braided Silk nonresorbable suture (SP118, Surgical Specialties Corporation). The pressure inside the balloon was increased at a rate of 15 mmHg/s until template rupture.

Sterilization of Template Samples

Templates were sterilized using a previously reported, lab-validated protocol [45]. Prior to the elution studies and cell-seeding with neutrophils, 8 mm biopsy punches (cat. no. P825, Acuderm Inc., Ft. Lauderdale, FL, United States) were taken from 4 individual templates of each Manuka honey concentration. In a sterile biosafety cabinet, templates were placed in a sterile 96-well plate (cat. no. 130188, Thermo Fisher Scientific) and positioned at a working distance of 9.5 cm beneath an 8-W, 365 nm wavelength lamp (cat. no. EN280L, Spectroline, Westbury, NY, United States) for 10 minutes on each side.

Manuka Honey Elution and Release Profile

Templates were then incubated in 200 µL of sterile Phosphate Buffered Saline (PBS, pH 7.4, cat. no. 10010-023, Gibco) for 1, 3, 6, and 24 hours, and 2, 3, 7, 14, and 21 days, at 37 °C and 5% CO_2 in a sterile incubator. At each time point, the supernatant was collected from each sample in 1.5 mL microcentrifuge tubes (cat. no. PR-MCT15, MidSci, Fenton, MO, USA) and stored at - 20 °C until analysis. The sample wells were replenished with 200 µL of PBS and returned to incubation. Collected samples were thawed for use in a colorimetric glucose assay (Glucose Assay Kit, Sigma Aldrich, cat. No. MAK476), and the absorbance was read on a SpectraMax i3x Multi-Mode Microplate Reader (Molecular Devices, San Jose, CA, USA) at 570 nm according to assay manufacturer instructions. The glucose concentration was determined from a glucose standard curve ranging from 0 to 300 µM of glucose, and correlated with a standard dilution of Manuka honey, ranging from 0.039% to 10%, which was assayed in tandem with the sample data. Data were reported as cumulative mean glucose concentration per sample per time point (n = 4).

NETosis Assay Via MPO ELISA on Neutrophil Supernatant

Five separate experiments were conducted using fresh peripheral blood neutrophils isolated from individual healthy donors of randomized race and sex (3 female, 2 male). Exclusion criteria for blood donation included autoimmune, endocrine, cardiovascular, or inflammatory diseases, as well as tobacco use. Donors were instructed to avoid alcohol consumption and non-steroidal anti-inflammatory drug (NSAID) use within 48 hours and were fasted for at least 12 hours prior to the blood draw appointment [19, 46, 47]. Donor selection, blood draw appointments, experiments, and donor data storage and protection followed protocols approved by the University of Memphis Institutional Review Board (IRB ID: PRO-FY2020-230), including informed consent.

Neutrophils were isolated from whole blood using a published, well-validated density separation protocol [19, 48, 49]. Blood was collected into EDTA-coated vacutainers (BD, Franklin Lakes, NJ, USA, ref. no. 366643) and donor autologous serum was collected in a separate untreated serum tube (BD, ref. no. # 366668). Blood was allowed to sediment gravitationally into white blood cell and red blood cell segments. The white blood cell segment was gently aspirated and centrifuged at 200 × g for 10 minutes at room temperature using a Sorvall ST8 Centrifuge (Rotor ID: 75005701, Thermo Scientific, Waltham, MA, USA). The supernatant was discarded, and the pellet resuspended in PBS and overlaid onto 3 mL of Isolymph (CTL, Deer Park, NY, USA, density 1.077 ± 0.001 g/mL, ref. no. 759050). The blood cells and Isolymph were centrifuged at 300 × g for 40 minutes at room temperature using the Sorvall ST8 Centrifuge (Rotor ID: 75005701, Thermo Scientific) with brakes disabled (soft acceleration and deceleration). Monocytes were removed first, and the supernatant was aspirated. The pellet was then resuspended in a 4 °C hypotonic (0.2%) NaCl solution for 30 seconds to lyse the remaining red blood cells. Tonicity was restored with a 4 °C 1.6% NaCl solution. NaCl solutions were comprised of ACS grade Sodium Chloride (MP Biomedicals, Santa Ana, CA, USA, ref. no.194738) in sterile, endotoxin-free cell culture grade water (Cytiva, Marlborough, MA, USA, ref. no. SH30529.02). The lysed red blood cell and neutrophil solution was then centrifuged at 200 × g for 7 minutes at 4 °C using a Sorvall ST8 Centrifuge (Rotor ID: 75005701, Thermo Scientific), then resuspended and washed in ice-cold PBS. Isolated neutrophils were then resuspended in 4 °C HBSS (Gibco, ref. no. 14175-095), containing 0.2% autologous human serum and 10 mM N-2-hydroxyethylpiperazine-N-2-ethane sulfonic acid (HEPES, Corning, Corning, NY, USA, ref. no. 25-060-CI) (referred to as HBSS+). Cell count and viability were analyzed via 0.4% Trypan blue (Gibco, ref. no. 15250-061) stain exclusion and a Countess II FL automated cell counter.

100 µL of the resuspended cell solution containing one million neutrophils per mL in HBSS+ was seeded onto sterilized and pre-wetted (40 µL of HBSS+ was added to each well after the templates were placed) biomaterials (n = 3) in a BioLite 96-well plate (Fisher). To ensure all wells had an equivalent final volume of 150 µL, negative tissue culture plastic (TCP) wells (n = 3) received 40 µL of HBSS+, and positive control TCP wells (n = 3) received 30 µL of HBSS+ prior to cell seeding. 10 µL of heparin (cat. no. H3393, Sigma–Aldrich, St. Louis, MO, United States) at a final concentration of 10 U/mL heparin was added to all wells to dissociate NET-associated MPO [24]. Negative control groups were left untreated, and the positive control wells were stimulated with 100 nM phorbol 12-myristate 13-acetate (cat. no. P8139, Sigma–Aldrich, St. Louis, MO, United States). All samples were incubated at 37 °C and 5% CO_2 for 4 hours. The 96-well plates were then placed on ice for 10 min to cease neutrophil activity during supernatant collection. 60 µL of fluid from each well was collected in 1.5 mL microcentrifuge tubes and centrifuged for 5 minutes at 500 × g at room temperature in a Sorvall Legend XTR Centrifuge (Rotor ID: 6133415, Thermo Scientific). 60 µL of the cell culture supernatant from each tube was then transferred to new microcentrifuge tubes and stored at -20 °C until analysis [50]. NET release was quantified using a human MPO enzyme-linked immunosorbent assay (Cat. No. BMS2038INST, ThermoFisher Scientific, Waltham, MA, USA) on a SpectraMax i3x Multi-Mode Microplate Reader (Molecular Devices). This method to quantify NET

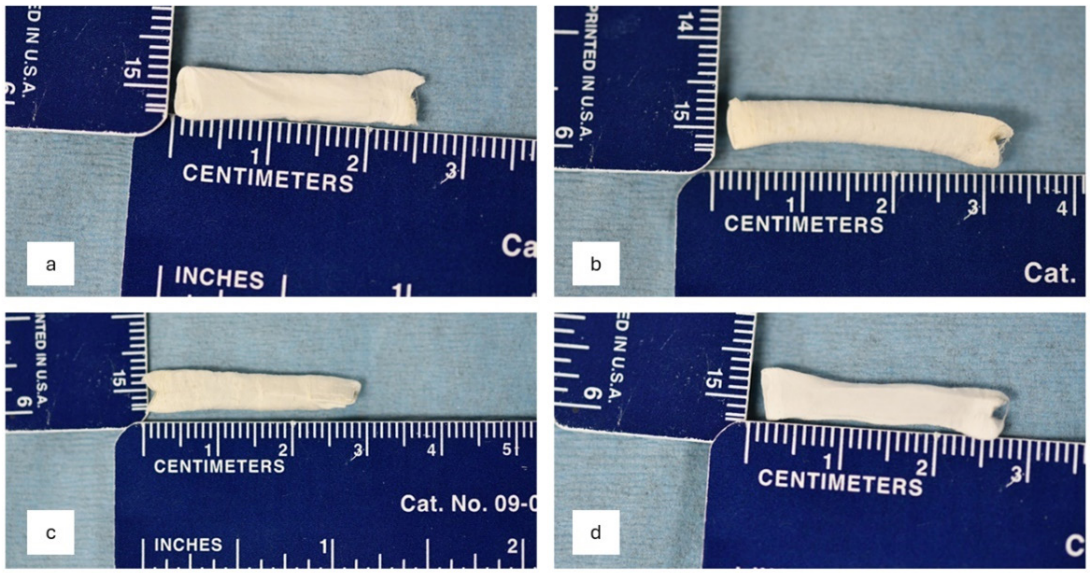

FIG. 4. Images of entire touch-spun (a) 0% MH (10% DI Water) template, (b) 0.1% Manuka honey template, (c) 1% Manuka honey template, and (d) 10% Manuka honey template immediately upon removal from the touch spinning mandrel.

release in response to biomaterial exposure has been lab-validated and published [50]. Data were normalized to the positive controls for each donor and expressed as the mean percentage of NETs per template.

SEM Imaging of Neutrophils on Biomaterial Interfaces

Neutrophils were isolated and cultured on biopsy punches of the touch-spun biomaterials using the previously described methods. After placing the 96-well plates on ice, the plates were centrifuged for 5 minutes at 500 × g at room temperature in a Sorvall Legend XTR Centrifuge (Rotor ID: 6133415, Thermo Scientific), and as much surrounding fluid was removed. Cells adherent to templates were fixed with 4% glutaraldehyde (Cat. No. 501840623, Fisher) in PBS, pH 7.4 (Gibco), for 18 hours at 4 °C. Prior to electron microscopy, the plates were centrifuged for 5 minutes at 500 × g at room temperature in a Sorvall Legend XTR Centrifuge (Rotor ID: 6133415, Thermo Scientific), and residual glutaraldehyde solution was removed. Then, templates and cells were dehydrated using increasing concentrations of 200-proof ethanol (Cat. No. AC615100010, Fisher) diluted with deionized water. Briefly, templates and adherent cells were treated with 100 µL of each corresponding concentration, and allowed to dry completely: 30%, 50%, 70%, 80%, 90%, 95% (twice), 99% (twice), and 100% ethanol (twice). As an alternative to critical-point drying, templates and cells were then dried using hexamethyldisilazane (HMDS, Cat. No. 440191, Sigma-Aldrich) diluted in 200-proof ethanol at the following concentrations: 25%, 50%, 75%, and 100% (twice) and allowed to dry completely. Templates and cells were transported in sealed containers in 100% HMDS, which was evaporated immediately prior to sputter coating and microscopy [51, 52]. Samples were sputter-coated and imaged using the same methods previously described.

Statistical Analysis and Data Visualization

All data were normalized, and the release study data were visualized in Microsoft Excel (Version 2405, Microsoft Corporation, Redmond, WA, USA). All data were tested for normality using the Shapiro-Wilk test and Q-Q Plots. All other differences were tested with ANOVA and Holm-Sidak's multiple comparisons tests. Statistical analyses and data visualization were performed in Prism version 8.4.3 (GraphPad Software, San Diego, CA, USA) at a significance level of 0.05. Fiber diameter and wall thickness data are reported as mean ± standard deviation. Mechanical testing and MPO ELISA data are reported as box-and-whisker plots showing the median, quartiles, and range, with individual sample or donor data overlaid as dots.

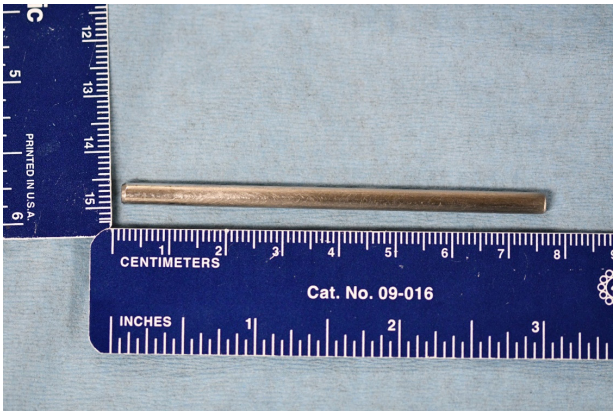

FIG. 5. 316L stainless steel mandrel used as the collection point for touch-spun fibers.

Results

Touch-spinning and Sample Preparation

FIG. 4 illustrates the touch-spun samples immediately upon removal (via sliding) from the polished 4 mm stainless steel mandrel (FIG. 5). It should be noted that for all uniaxial mechanical testing, suture retention, burst pressure, Manuka honey release study, and neutrophil MPO release, the middle sections (5 mm in from each end) were used.

Biomaterial Characterization

Based on ImageJ analysis of SEM images (FIGs 6 and 7) and digital caliper measurements prior to mechanical testing (TABLE 1), 0% and 1% Manuka honey concentrations had

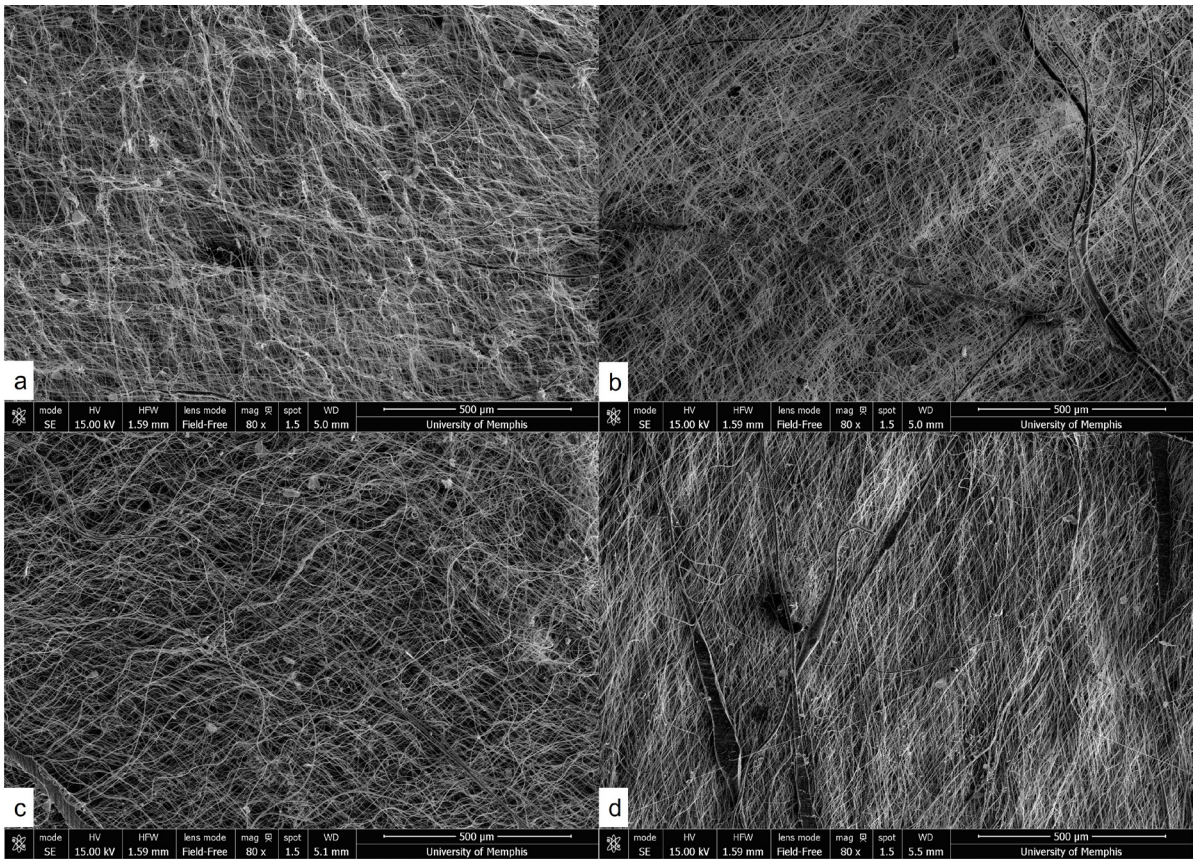

FIG. 6. Representative 80× SEM images of the outer surface of the (a) 0% MH (10% DI Water) template, (b) 0.1% Manuka honey template, (c) 1% Manuka honey template, and (d) 10% Manuka honey template. Scalebars = 500 µm.

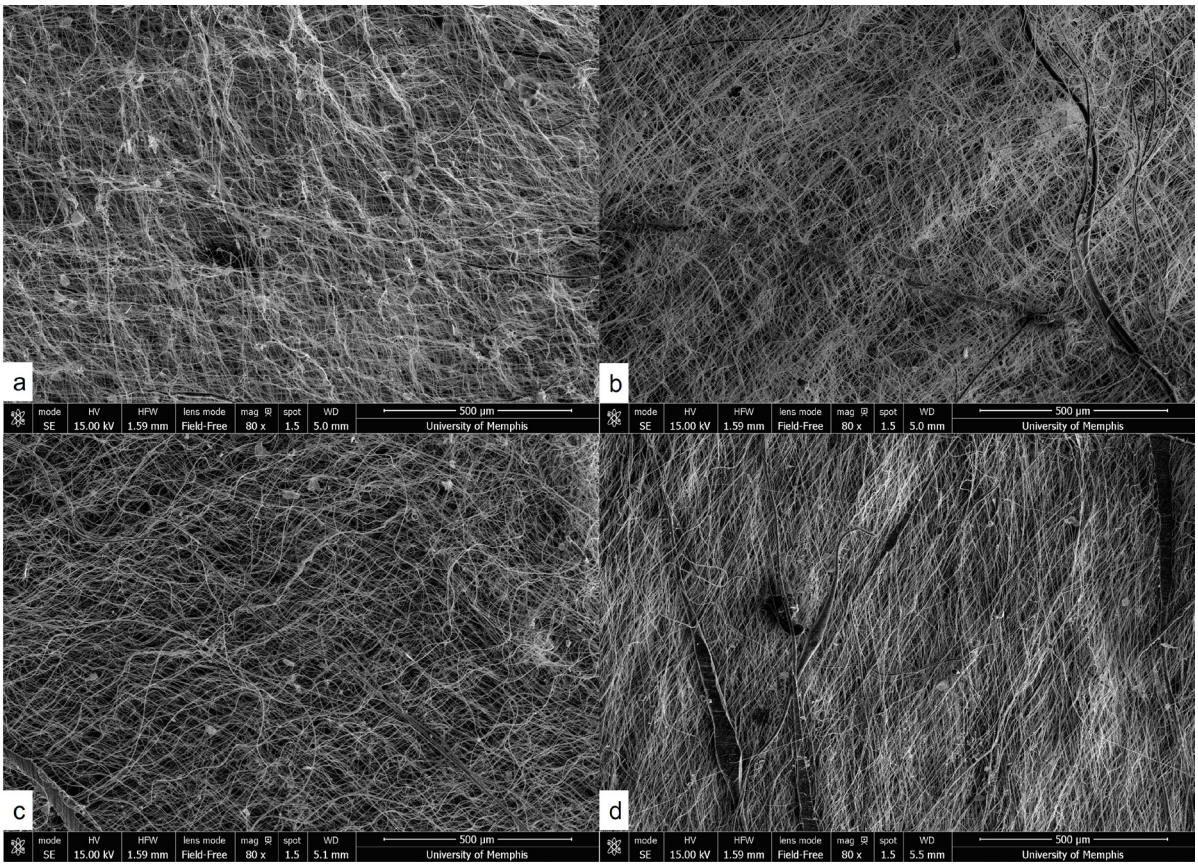

FIG. 7. Representative 500× SEM images of the outer surface of the (a) 0% MH (10% DI Water) template, (b) 0.1% Manuka honey template, (c) 1% Manuka honey template, and (d) 10% Manuka honey template. Scalebars = 50 µm.

TABLE 1. Fiber Diameter and Wall Thickness of Touch-Spun Templates

	Fiber Diameter (μm)	Wall thickness (μm)
0% Manuka Honey	1.006 ± 0.533	230 ± 78
0.1% Manuka Honey	1.453 ± 0.221	150 ± 24
1% Manuka Honey	1.042 ± 0.621	108 ± 46
10% Manuka Honey	1.263 ± 0.588	135 ± 23

somewhat lower fiber diameters but remained within 1 standard deviation of the other groups. Similarly, 0% Manuka honey had a larger mean wall thickness, but its standard deviation overlapped with those of other sample groups. All touch-spinning parameters were conserved between sample groups. No detectable morphological changes, including Manuka honey-based crystallinity, were observed in the SEM images, as some crystalline structures were observed in all image groups, even in 0% Manuka honey. These crystalline structures, observed at the surface-facing levels of the biomaterial, are likely attributable to polymer debris or environmental dust, introduced during processing and SEM imaging preparation.

Ultimate Tensile Strength

The ultimate tensile strength (UTS) of each template was measured in both the longitudinal and circumferential axes. Along the longitudinal axis, the UTS of the 10% concentration was lower than the other templates. The 10% concentration templates had a UTS of 0.67 ± 0.10 MPa, while the 0.1% templates had a UTS of 2.38 ± 0.81 MPa, the 1% templates had a UTS of 2.44 ± 0.34 MPa, and the 10% water templates had a UTS of 2.40 ± 0.56 MPa. Along the circumferential axis, the UTS of the 10% concentration templates was again lower than the other template values with a mean of 2.44 ± 0.82 MPa. The UTS of the 10% Manuka honey templates was 2.44 ± 0.82 MPa, while the UTS of the 0.1% templates was 5.10 ± 2.82 MPa, the 1% templates was 5.88 ± 2.49 MPa, and the 10% water templates was 5.59 ± 3.63 MPa. In summary, all touch-spun template ultimate tensile strengths were statistically significantly different from the saphenous vein and internal mammary artery values ($p<0.0001$) in the longitudinal direction (FIG. 8a), but matched both the saphenous vein and internal mammary artery values closely in the circumferential direction (FIG. 8b).

Percent Elongation

The percent elongation of each template was also measured in both the longitudinal and circumferential axes. Along the longitudinal axis, the percent elongations were similar and greater than both the IMA and SV values. The 0.1% concentration templates had a percent elongation of 171.8 ± 46.5%, the 1% concentration 167.7 ± 14.8%, the 10% concentration 139.2 ± 20.1%, and the 10% water concentration 181.5 ± 14.2%. Along the circumferential axis, the percent elongation values were closer to the SV reference value. The 0.1% concentration templates had

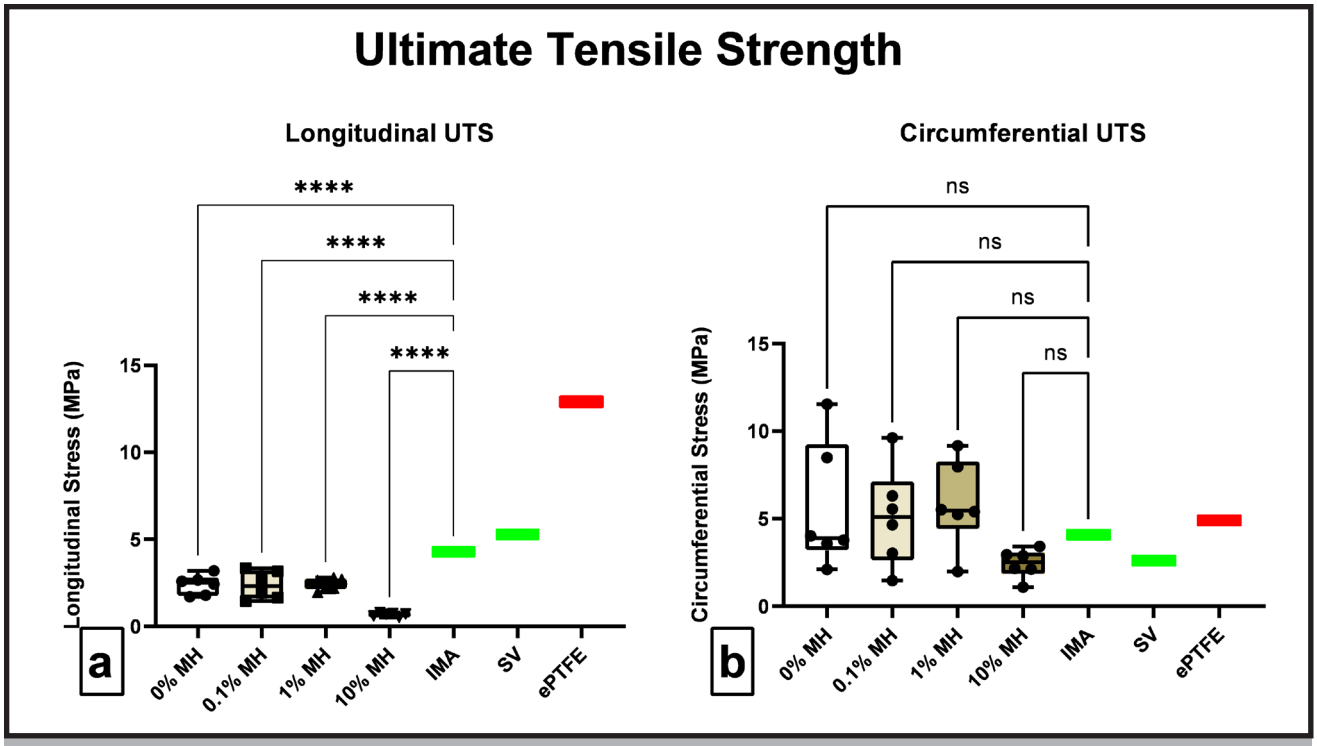

FIG. 8. Ultimate tensile strength of touch-spun vascular grafts along (a) the longitudinal axis and (b) the circumferential axis (boxplots represent median and quartiles, whiskers represent range, and dots represent individual data sample values (n = 6), red bar indicates literature values for Gore-Tex® ePTFE vascular grafts, green bars indicate literature values for SV and IMA). Quadruple asterisks indicate a p-value below 0.0001. Label "ns" indicates no statistical significant difference.

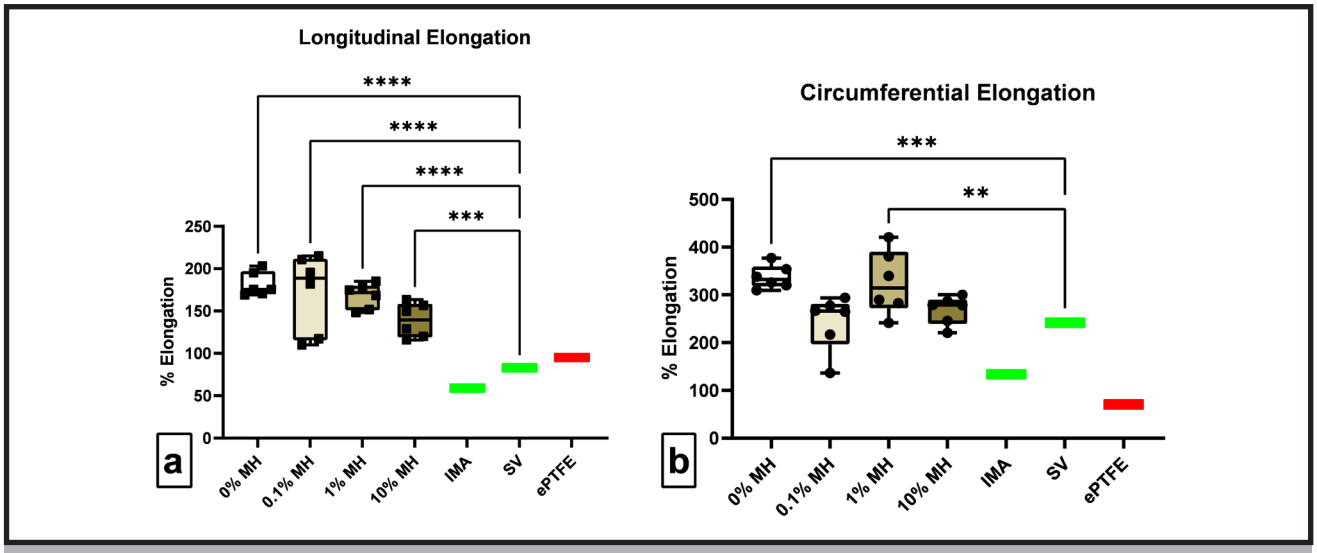

FIG. 9. Percent elongation of touch-spun vascular grafts along (a) the longitudinal axis and (b) the circumferential axis (boxplots represent median and quartiles, whiskers represent range, and dots represent individual data sample values (n=6), red bar indicates literature values for Gore-Tex® ePTFE vascular grafts, green bars indicate literature values for SV and IMA). Triple asterisks indicate a p-value below 0.001, quadruple asterisks indicate a p-value below 0.0001.

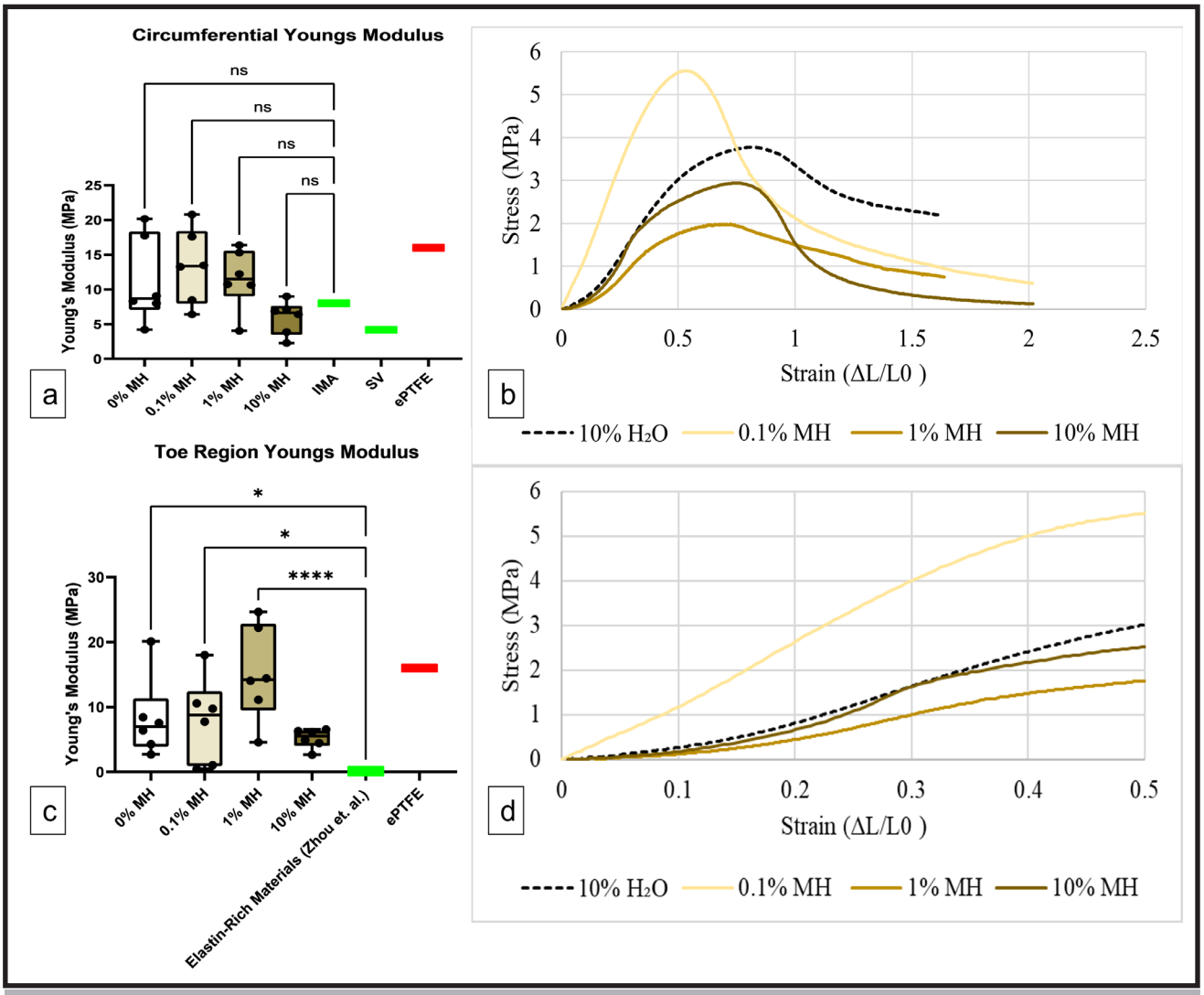

FIG. 10. Young's modulus of touch-spun vascular grafts along the circumferential axis (a) (boxplots represent median and quartiles, whiskers represent range, and dots represent individual data sample values (n=6), red bar indicates literature values for Gore-Tex® ePTFE vascular grafts, green bars indicate literature values for SV and IMA). Label "ns" indicates no statistical significant difference. Stress-strain curves of touch-spun vascular grafts (b). Young's modulus within the toe-region of touch-spun vascular grafts along the circumferential axis (a) (boxplots represent median and quartiles, whiskers represent range, and dots represent individual data sample values (n=6), red bar indicates literature values for Gore-Tex® ePTFE vascular grafts, green bars indicate literature values for toe-region Young's modulus for elastin-rich materials).

a percent elongation of 242.7 ± 51.2%; the 1% concentration, 325.9 ± 67.1%; the 10% concentration, 268.5 ± 29.6%; and the 10% water concentration, 337.6 ± 24.8%. In a similar fashion to ultimate tensile strength, all touch-spun templates failed to match longitudinal saphenous vein and internal mammary artery values (FIG. 9a). However, in the circumferential direction, 0.1% and 10% Manuka honey templates were closely aligned with saphenous vein values (FIG. 9b).

Young's Modulus

The Young's modulus was calculated along the circumferential axis. Among all template groups, only the 10% MH concentration aligned between the SV and IMA reference values at 5.95 ± 2.43 MPa. The Young's modulus was calculated as 13.35 ± 5.39 MPa for the 0.1% concentration templates, 11.57 ± 4.38 MPa for the 1% concentration, and 11.27 ± 6.25 MPa for the 0% Manuka honey templates. All touch-spun templates demonstrated Young's modulus values similar to those of the internal mammary artery, with 10% Manuka honey most closely matching (FIG. 10a). The data suggest a Manuka honey concentration-dependent reduction in Young's modulus. The stress-strain curves, upon qualitative analysis, revealed a J-curve trend for touch-spun templates (FIG. 10b). This J-curve is similar to the native IMA and SV values in prior literature, and the toe region slopes are between those of elastin-rich tissues and ePTFE vascular grafts [44, 53]. Analysis of the stress-strain curves revealed the toe region Young's modulus values for the 0% Manuka honey, 0.1% Manuka honey, 1% Manuka honey, and 10% Manuka honey touch-spun templates to be 8.25 ± 6.18 MPa, 7.94 ± 6.55 MPa, 15.18 ± 7.35 MPa, and 5.18 ± 1.49 MPa, respectively (FIG. 10c). The toe region was defined empirically as the region between strain values of 0.2-0.5 for the given data set (FIG. 10d).

Suture retention

The suture retention measured the maximum load of a suture through one wall of the graft. The maximum load of the suture was 206.89 ± 69.62 gf for the 0.1% concentration, 144.44 ± 45.07 gf for the 1% concentration, 97.58 ± 36.40 gf for the 10% MH concentration, and 20.05 ± 3.20 gf for the 0% Manuka honey concentration. The only sample group to fail to meet the internal mammary artery values was the 0% Manuka honey, while the 0.1% Manuka honey exceeded the value. The data presented suggest that incorporation of Manuka honey enhances the ability of touch-spun vascular templates to meet autologous blood vessel suture retention values, particularly at lower concentrations (FIG. 11).

Burst Pressure

The calculated burst pressure values for both Manuka honey concentration groups and the 0% control fell similarly well below the IMA and SV reference values, with values of 484.4 ± 77.8 mmHg for the 0.1% concentration group, 491.2 ± 83.1 mmHg for the 1% concentration group, 431.5 ± 78.1 mmHg for the 10% MH concentration group, and 453.7 ± 133.3 mmHg for the 0% Manuka honey group (FIG. 12). All touch-spun vascular templates failed to meet the literature values for internal mammary artery and saphenous vein burst pressures ($p<0.0001$).

Manuka Honey Elution and Release Profile

Data from the glucose assay demonstrated that, as expected, 0% Manuka honey templates did not elute detectable glucose, whereas all sample groups containing Manuka honey eluted glucose at a concentration that could be converted to mg/mL Manuka honey via comparison to a standard curve of Manuka honey dilutions assayed in the same glucose assay plate. The 0.1% Manuka honey templates eluted all of their Manuka honey within the first hour of incubation, reaching a final value of 5 mg/mL. The 1% templates eluted all of their Manuka honey by day 2 of incubation, reaching a final value of 20 mg/mL (FIG. 13a). 10% Manuka honey templates eluted all of their Manuka honey by three days of incubation, at a final elution concentration of 15 mg/mL Manuka honey (FIG. 13b). Surprisingly, the 1% Manuka honey templates eluted consistently 5 mg/mL more Manuka honey than the 10% group templates, with a higher release profile beginning in the first hour of incubation under physiological conditions.

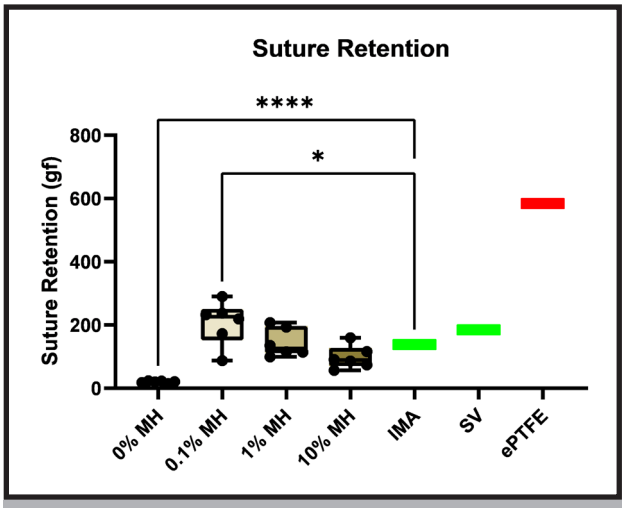

FIG. 11. Suture retention of touch-spun vascular grafts along the longitudinal axis (boxplots represent median and quartiles, whiskers represent range, and dots represent individual data sample values (n = 6), red bar indicates literature values for Gore-Tex® ePTFE vascular grafts, green bars indicate literature values for SV and IMA). Single asterisk indicates a p-value below 0.05, quadruple asterisk indicates a p-value below 0.0001.

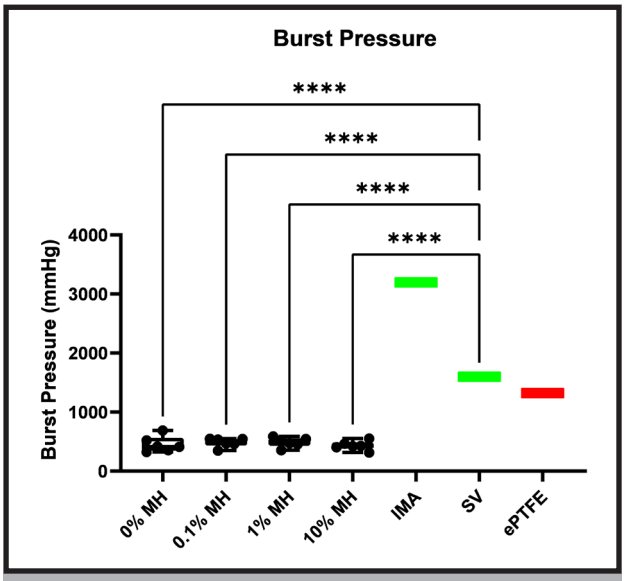

FIG. 12. Burst pressure of touch-spun vascular grafts (boxplots represent median and quartiles, whiskers represent range, and dots represent individual data sample values (n = 6), red bar indicates literature values for Gore-Tex® ePTFE vascular grafts, green bars indicate literature values for SV and IMA). Quadruple asterisk indicates a p-value below 0.0001.

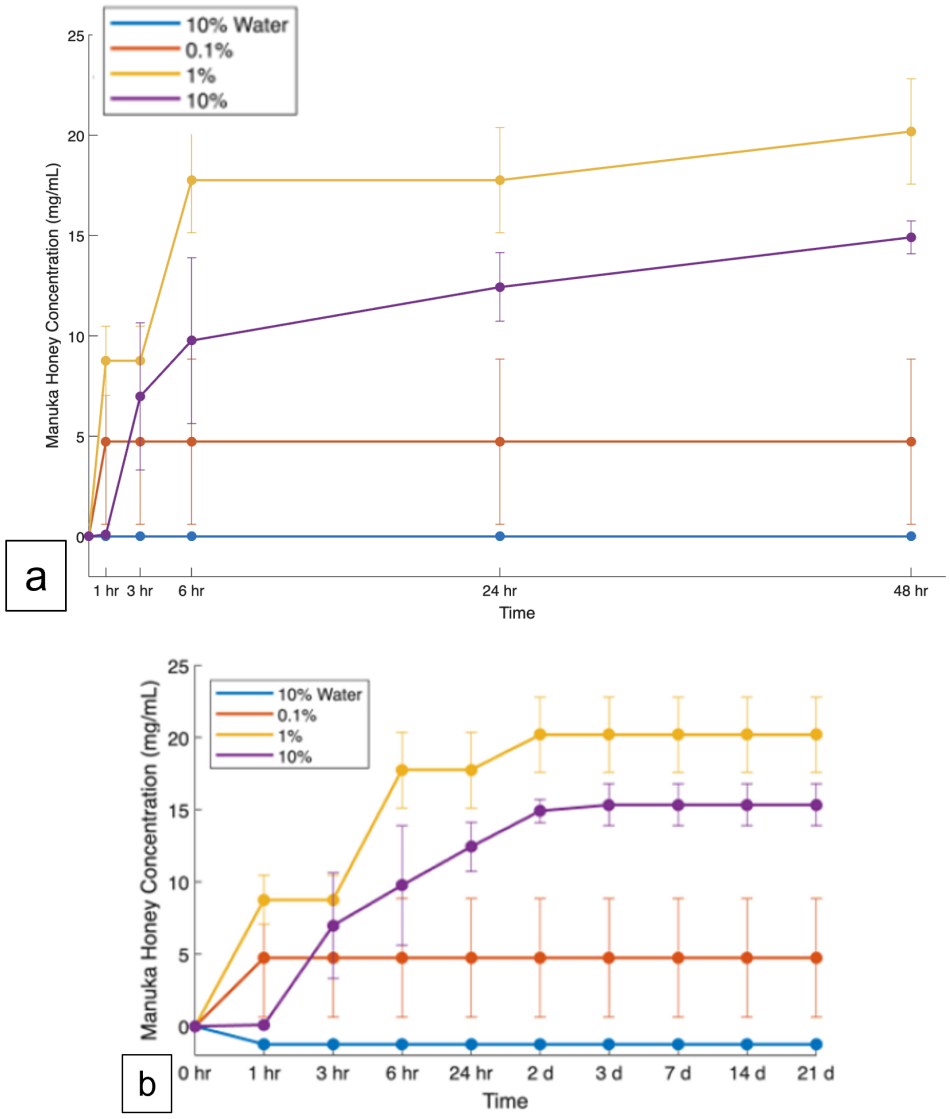

FIG. 13. Manuka honey cumulative elution of touch-spun vascular grafts within (a) the first 48 hours and (b) throughout the 21-day length of the study (dots represent sample value means, error bars indicate standard deviation (n=4)).

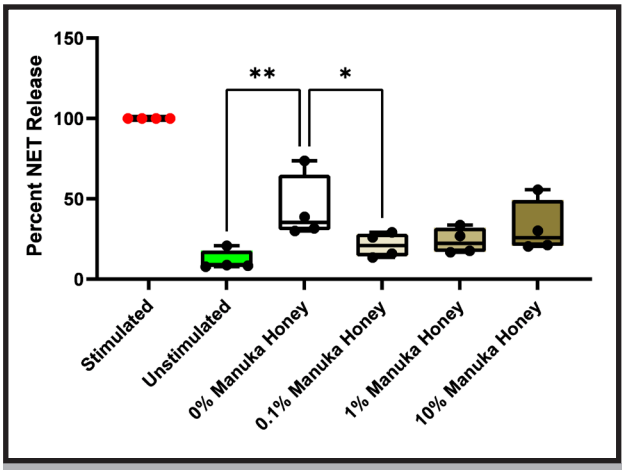

FIG. 14. NET release from stimulated neutrophils (positive control shown in red), unstimulated, resting state neutrophils (negative control, shown in green), and touch-spun vascular grafts. Data presented as percentage of the mean stimulated control level of MPO (boxplots represent median and quartiles, whiskers represent range, and dots represent individual data sample values (n=4). Asterisk indicates a p-value below 0.05, double asterisk indicates a p-value below 0.01.

NETosis Assay Via MPO ELISA on Neutrophil Supernatant

The data from the MPO assay demonstrated that unstimulated (no PMA added to the culture media) neutrophils had a mean MPO release of 11.45% of the positive PMA-treated control cells, indicating sufficient and reliable stimulation of NETosis by PMA. 0% Manuka honey vascular templates had a mean MPO release of 43.60% compared to positive control, 0.1% Manuka honey templates had a mean MPO concentration of 21.17% of positive control, 1% Manuka honey had 23.78% of the MPO levels of positive control cells, and 10% Manuka honey templates had 31.91% of MPO release compared to the positive control (FIG. 14). All sample groups were significantly different from the positive control. The only touch-spun sample group to be statistically significantly different from baseline unstimulated levels was the 0% Manuka honey template, while the 0.1% Manuka honey templates were statistically significantly lower than the 0% group. Surprisingly, no dose-dependency was observed: 0.1% and 1% concentrations were most effective at reducing neutrophil NETosis, whereas 10% Manuka honey was less effective.

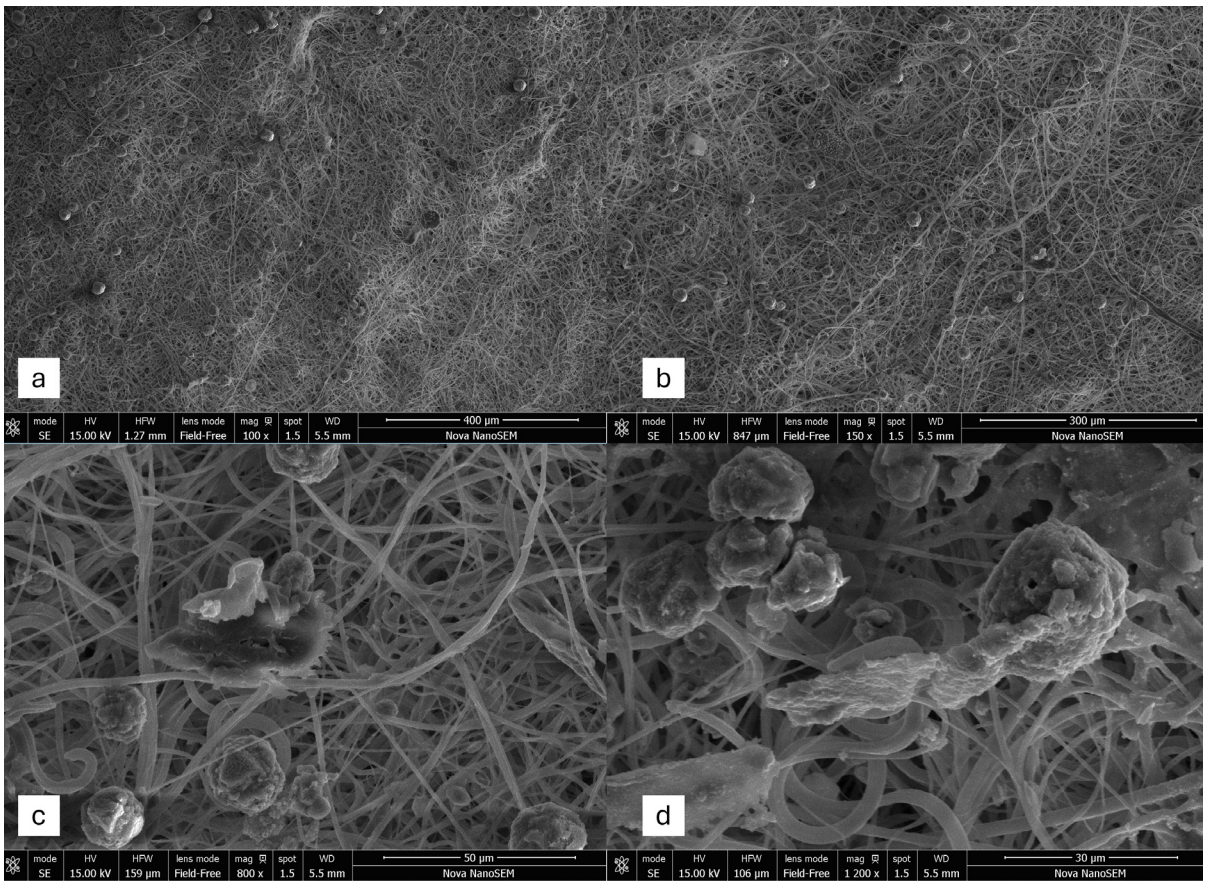

FIG. 15. Representative SEM images of neutrophils adherent to the outer surface of the 0% MH (10% DI Water) touch-spun templates at 100× (a), 150× (b), 800× (c), and 1200× (D). Scalebars = 400 µm, 300 µm, 50 µm, and 30 µm, respectively.

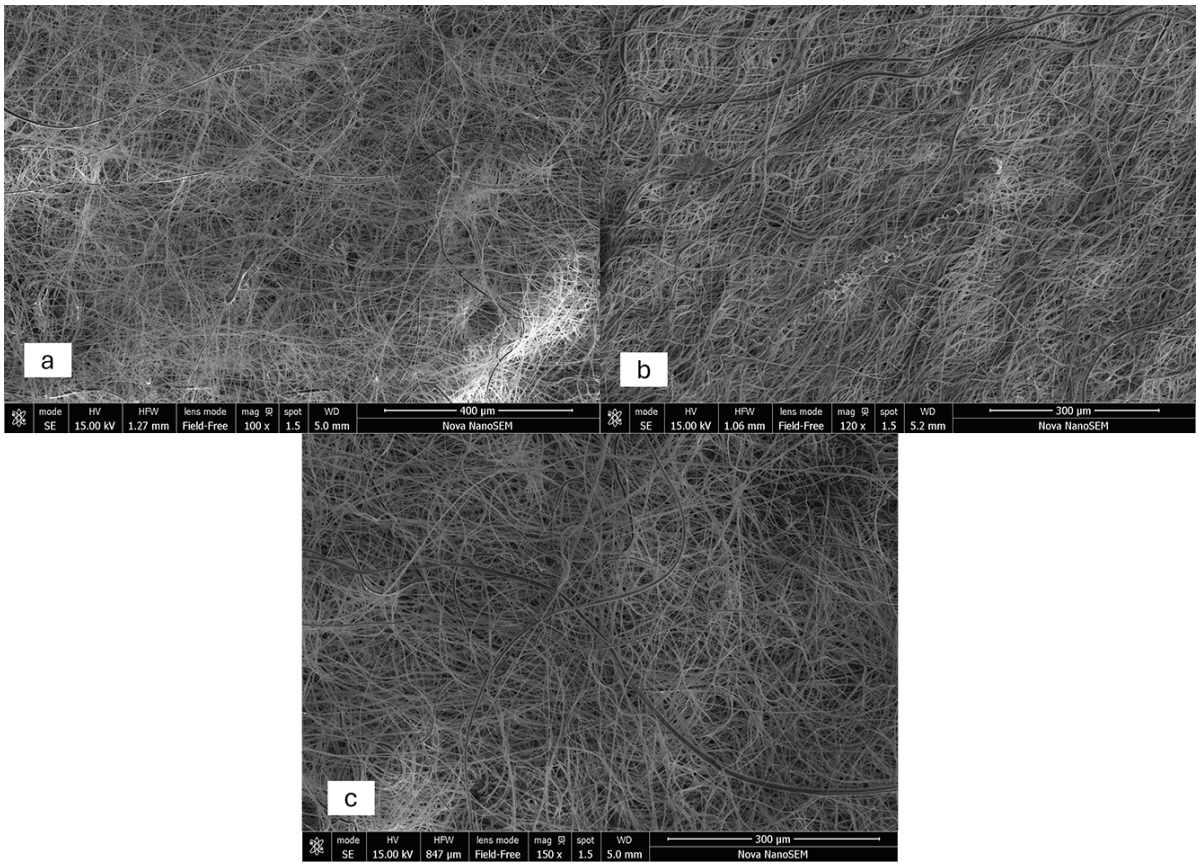

FIG. 16. Representative SEM images of a lack of neutrophils adherent to the outer surface of the 0.1% MH touch-spun templates at 100× (a), 1% MH touch-spun templates at 150× (b), 1% MH touch-spun templates at 150× (c). Scalebars = 400 µm, 300 µm, and 300 µm, respectively.

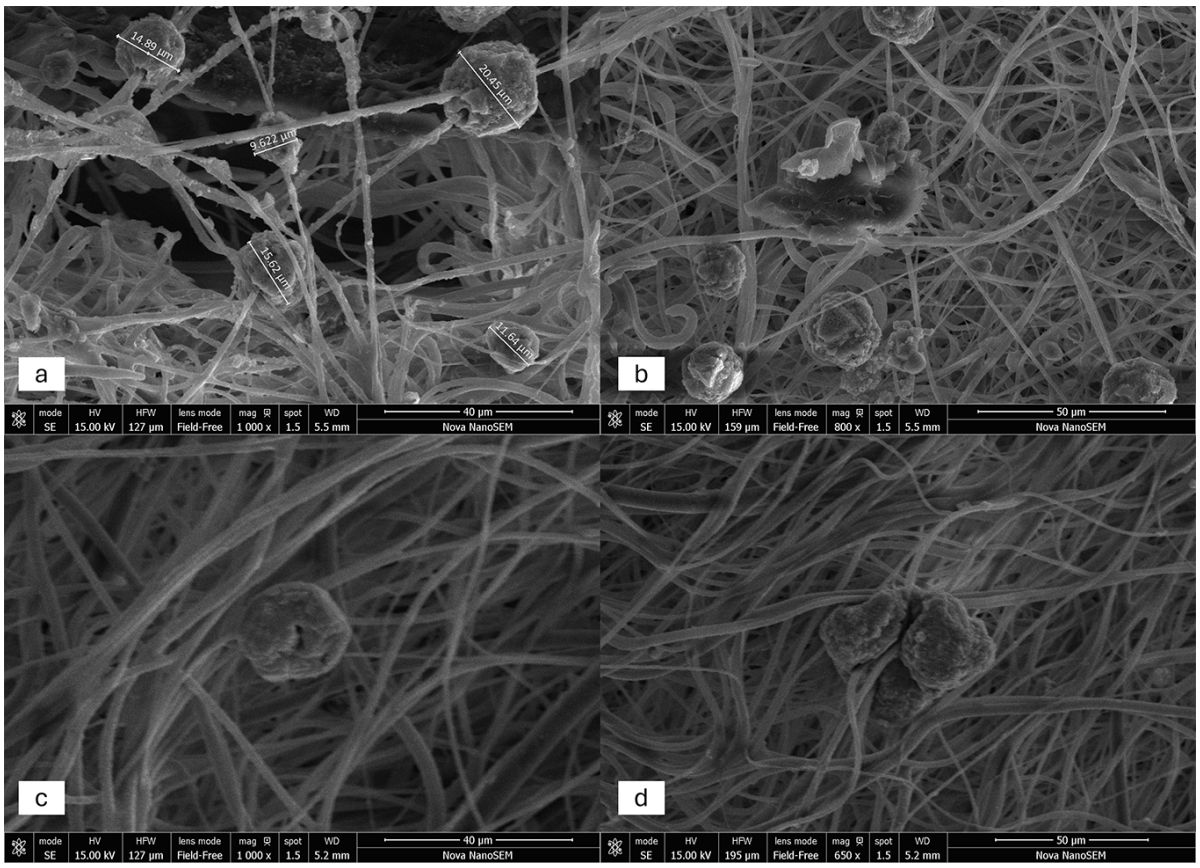

FIG. 17. Representative SEM images of distinguishing neutrophil morphology at the outer surface of the 0% MH touch-spun templates at 1000× (a), 800× (b), and on 1% MH touch-spun templates at 1000× (c) and 650× (d). Scalebars = 40 µm, 50 µm, 40 µm, and 50 µm, respectively.

Consistent with the MPO data, SEM micrographs revealed increased neutrophil adhesion and NET-like morphological characteristics in the 0% Manuka honey templates (FIG. 15) compared to the 0.1%, 1%, and 10% templates (FIG. 16). Interestingly, neutrophil NETosis has not been abundantly analyzed, especially at fibrous biomaterial interfaces, using SEM due to the fragility of the DNA and histone nanofibers. As such, it is difficult to compare images to conclusively state what neutrophil NETosis looks like in this context. FIG. 17 shows neutrophil morphologies of interest, including what appears to be adhesion to multiple fibers at a time, the ejection of intracellular components, and multiple neutrophils engulfing fibers at the same point.

Discussion

ePTFE, patented in 1969 by W.L. Gore, has been the gold standard of synthetic vascular graft materials for the past 54 years. One of the only changes made since this time has been heparin surface modifications to lower thrombogenicity, which have had limited success and yielded outcomes similar to those of unmodified ePTFE [54]. Tissue engineering and regenerative medicine approaches have been attempted over the past 30+ years with promising results compared to ePTFE. Several of these studies aim to address patency issues caused by poor tissue integration and have developed an in-situ tissue-engineering approach using the body as a bioreactor. These approaches use decellularized donor tissue or ECM, or biodegradable polymers, as templates for cells to adhere to and remodel, with the ultimate goal of being replaced by functional vascular tissue [55, 56]. Decellularized matrices have shown promise, with limited immunological response and acceptable outcomes in patients nine months after arteriovenous fistula implantation for dialysis access. However, the utilization of decellularized tissue is laborious, time-consuming, and expensive [57]. The use of synthetic polymers circumvents these limitations and has shown initial promise for mechanical properties, but key limitations remain. In many cases, fibrous encapsulation and a significant foreign body response occur, rendering meticulously curated porosity, mechanical properties, and surface properties of these biomaterial designs ineffective. These limitations are related to the initial neutrophil response to foreign materials and the inability to resolve the acute phase of inflammation. Rampant neutrophil inflammatory activity and recruitment to the implant site shift the host-biomaterial continuum towards wound closure and foreign object isolation, in which the body walls off the foreign material (the biomaterial implant) with a fibrous capsule [9, 10]. There has been recent interest in immunomodulatory biomaterials that aim to quell the foreign body reaction. Yet, few studies have targeted modulating the acute phase of inflammation to achieve higher device success rates, and even fewer still focus on targeting neutrophil inflammatory behavior (a majority of which have come from this lab in recent years) [58-61]. An inappropriate neutrophil response to an implant can have deleterious cascading effects, ultimately leading to device failure. However, to date, limited investigation has been conducted into novel fabrication techniques, therapeutics, and additives that can be incorporated into biomaterial designs to reduce the acute-phase host immune responses and enable tissue regeneration.

Thus, the current lack of synthetic small-diameter vascular grafts on the market, driven by poor patency and high device failure rates, is mainly due to their inability to quell the initial acute inflammatory response to implantation. Revascularization therapies involving vessel diameters lower than 6 mm, which are dependent on autologous vein

transplantation, cause morbidity at the site where donor blood vessels are extracted and are often of poor quality due to the progression of cardiovascular disease within the donor blood vessel. Thus, the lack of viable synthetic options in the clinic contributes to cardiovascular disease's increasingly high worldwide mortality rate, the 1 million limbs worldwide amputated yearly, and negatively impacts the efficacy of over 400,000 coronary bypass surgeries performed in America alone. [11].

The primary issues plaguing vascular grafts, especially small-diameter grafts, are hyperplasia, thrombosis, infection, and atherosclerosis [11]. Key upstream factors that cause these effects include the rampant oxidative and enzymatic degradation of the device-tissue interface by neutrophils during the acute inflammation stage, the perpetuation of the inflammatory response due to a persistent pro-inflammatory microenvironment, and, ultimately, fibrous encapsulation. The failure of a vascular graft to resolve acute inflammation shifts the course of healing towards isolation and attempted removal (fibrous encapsulation) rather than regeneration (tissue integration with the porous graft). Therefore, this shift away from regeneration dooms the device to hyperplasia, thrombosis, and atherosclerosis due to flow disturbances caused by the fibrous encapsulation, which occludes the vessel and creates a mechanical mismatch at the site of anastomosis. Thus, our investigation sought to leverage the anti-inflammatory properties of Manuka honey to reduce neutrophil-mediated inflammation during small-diameter vascular graft implantation and thereby improve the resulting host-biomaterial interaction, thereby reducing the risk of fibrous encapsulation while maintaining the mechanical properties sufficient to meet the needs of a vascular prosthetic.

As in prior reports on the incorporation of Manuka honey into fibrous templates, no meaningful differences in morphology, fiber diameter, or wall thickness were observed between Manuka-honey-incorporated and control templates. These findings are crucial, as wall thickness is closely linked to mechanical properties, and fiber diameter has been shown to influence the immune response to electrospun templates [24, 29, 48]. These findings are also important because the total surface area-to-volume ratio and fiber architecture are closely linked to release profiles and could affect the ability to gather meaningful data on Manuka honey release [58, 62]. While the wall thicknesses were relatively small compared to other fabrication methods, the mechanical properties, especially in the circumferential direction, exceeded expectations, with values matching or closely matching those of the native vasculature.

The ultimate tensile strength of the touch-spun templates showed an opportunity for further development, along with other mechanical properties in the longitudinal direction. However, the circumferential ultimate tensile strength closely matched that of the internal mammary artery, with higher Manuka honey concentrations bringing it directly between the saphenous vein and the internal mammary artery. All touch-spun template groups showed no statistically significant differences in circumferential ultimate tensile strength, showing tremendous potential of these grafts to match natural vasculature compliance and burst pressure.

Similarly to ultimate tensile strength, percent elongation values in the longitudinal direction did not meet the saphenous vein or internal mammary artery values regardless of Manuka honey incorporation. However, along the circumferential axis, only 0% and 1% Manuka honey templates showed statistically significant differences in percent elongation from saphenous vein literature values. Again, these findings show the need for development in the longitudinal properties of touch-spun templates, but a close matching in compliance and flexibility in the circumferential axis.

The Young's modulus values demonstrated the exceptional ability of touch-spun vascular grafts to match the mechanical properties of native vasculature. Circumferential Young's modulus values are especially important as they are closely related to vessel burst pressure, and in many investigations, especially *in vivo*, used as a direct allegory for this critical value [63]. It is important to note that with mechanical properties, it is not a matter of "bigger is better." Meeting, but not overly exceeding, the mechanical strengths of blood vessels is paramount, as failure to meet the values on the lower end can cause device rupture, but mechanical mismatch and overly stiff materials have been shown to cause hyperplasia, blood flow disturbances, and are associated with poor device outcomes [64].

In contrast to other mechanical properties measured along the longitudinal axis in this study, suture retention values for the touch-spun templates showed excellent mechanical properties, with all values nestled between literature values for the internal mammary artery and the saphenous vein. Only the 0.1% Manuka honey-incorporated touch-spun templates were statistically significantly different from the internal mammary artery. However, the 0.1% Manuka honey-incorporated samples were closely aligned to the suture retention values of the saphenous vein. These findings are important as they demonstrate that these templates can withstand the surgical procedure required for implantation and for proper healing at the site of anastomosis [65, 66]. The suture retention values for templates not incorporated with Manuka honey were markedly lower than those incorporating Manuka honey. This discrepancy is likely due to increased interfacial fusion between fibers and between successive fiber layers, thereby promoting fiber cohesion while maintaining porosity. Previous studies involving Manuka honey and biomaterial fabrication did not report increases in polymer crystallinity, which is in line with our morphological observations [24, 29].

Data from the burst pressure analysis indicated that the touch-spun templates alone did not meet the burst pressure values for the saphenous and internal mammary artery. In some ways, this is surprising, as the circumferential Young's moduli for native blood vessels and the touch-spun templates were closely matched, and Young's modulus is a critical determinant for burst pressure. However, this is not entirely surprising, considering that these are porous templates designed to allow cellular infiltration and transcapillary ingrowth, and that, in the clinic, they would require a pre-clotting or cell-seeding step. The data gathered from this investigation show significant promise in the mechanical properties of the materials and fabrication techniques themselves. However, further research is required on the mechanical properties post-preparation, specifically the burst pressure after the material is no longer porous and has been processed to be sufficiently water-tight and ready for implantation.

Surprisingly, the Manuka honey elution study demonstrated more overall Manuka honey release and a longer, more sustained release profile from the 1% Manuka honey templates. Both the 1% and 10% Manuka honey templates eluted within the first three hours of implantation and continued to steadily release Manuka honey for 2 days under stimulated physiological conditions. This timing is highly beneficial for the primary goal of this study, which was to develop small-diameter vascular grafts that aid in resolving the neutrophil-dominant acute phase of inflammation following implantation. This 48-hour timing coincides with the typical duration of an acute-phase inflammatory response to an implanted material [9, 10]. The steady release of Manuka honey throughout this time period means that as neutrophils are continually migrating via chemotaxis, interfacing, and responding to the implant, there is a steady release of

therapeutic Manuka honey to both prevent infection and quell neutrophil inflammatory behaviors such as ROS generation, NET release, and pro-inflammatory signaling [13, 19, 21, 61, 67]. While the current study was predominantly focused on the resolution of acute-phase inflammation and on the critical first few days to weeks post-implantation, the elution study extended to 21 days, with most of the honey measured eluting after 48 hours. However, particularly for the 10% Manuka honey templates, not all of the Manuka honey was eluted. Because all supernatants were retained and all measurements were cumulative, there was no possibility that Manuka honey could be washed away or discarded. Thus, the discrepancy between the quantity of Manuka honey incorporated into the biomaterial and the amount eluted is likely due to a retention of Manuka honey after the 21-day time point. This explanation is corroborated by other investigations involving the loading of antibiotics into PDO polymer templates. Researchers observed similar release kinetics, with most of the incorporated bioactive eluting over the first several days. However, as the polymer began to degrade, the templates eluted the remaining antibiotic over the course of weeks [68]. While the timing of Manuka honey release differs slightly from the previously mentioned study, a similar release profile could be observed in long-term (4-8 weeks) studies.

MPO, a critical enzyme released by neutrophils undergoing NETosis, has been used as a reliable marker for NETs at the interface of biomaterials to measure the neutrophil inflammatory response to biomaterial surface interactions [69]. Dysregulated NETosis and subsequent MPO release have been associated with a wide range of pathologies and are highly linked to poor biomaterial outcomes [18, 70, 71]. Far from being an inert marker used to quantify NETosis, MPO actively drives the respiratory burst phenomenon seen in neutrophil activation by using H_2O_2 to create hypohalous acid, hypochlorous acid, hypobromous acid, and hypothiocyanous acid. These compounds are potent oxidants and can be beneficial to clear bacterial infection, but when dysregulated, they can be highly cytotoxic [72]. Additionally, dysregulated MPO release from neutrophils contributes to a state of constituent neutrophil pro-inflammatory signaling, creating a vicious cycle of acute-phase inflammation at an implant site [73]. The influence of MPO in the case of vascular graft implantation is especially critical, as MPO has been directly linked to neointimal hyperplasia by reacting with H_2O_2 to activate smooth muscle cell proliferative pathways. Of note, MPO inhibitors or knockout treatments significantly reduced neointimal hyperplasia [74, 75]. Therefore, vascular tissue engineering templates pre-loaded with an MPO-inhibiting bioactive would be highly beneficial for reducing neointimal hyperplasia and stenosis.

In this study, it was demonstrated that touch-spun templates incorporating Manuka honey into the fibrous structure reduced MPO release from neutrophils in co-culture. Furthermore, all Manuka honey-incorporated template sample groups were not statistically significantly different from the negative control (non-stimulated neutrophils). Unsurprisingly, the touch-spun templates without Manuka honey showed higher MPO release than the Manuka honey groups and unstimulated neutrophils, but still at a level lower than expected based on traditional electrospinning reports [24, 48, 58]. These findings not only corroborate prior reports that Manuka honey incorporation into biomaterials prevents neutrophil NETosis but also suggest that these effects are enhanced when used in touch-spun biomaterials. Further, these data suggest that touch-spinning yields a template architecture that is less NET-inducing than traditional electrospinning, even without the incorporation of a therapeutic component.

Overall, this investigation elucidated three overall findings. First, Manuka honey can be incorporated into touch-spun small-diameter vascular grafts without significantly altering surface morphology, fiber diameter, or the overall mechanical properties that determine whether these fibrous templates are suitable as vascular prosthetics. Second, that Manuka honey, upon incorporation into the polymer solution and, in turn, into the templates' fibrous structures, will elute at therapeutically beneficial rates and concentrations over 1 hour (0.1%) to 2 days (1% and 10%). Third, and arguably the most important finding, is that touch-spun biomaterial templates incorporating Manuka honey reduce neutrophil NETosis to near-baseline levels, and even non-Manuka-honey-incorporated templates exhibit low to moderate NET levels compared with other biomaterial fabrication methods [24, 76].

The mechanical properties of the touch-spun templates were not affected by the incorporation of Manuka honey. However, compared to more recent advances in biomaterial fabrication techniques, the mechanical properties in the longitudinal direction could be improved [77]. The failure to meet the longitudinal ultimate tensile strength and percent elongation could be related to the overall wall thickness of the templates or the cross-hatching angles, both of which were held constant through this study. Previous reports show that the touch-spinning apparatus used for this study can modulate and control fiber spacing and alignment to tailor mechanical properties [32]. Further study is needed to determine which parameters should be adjusted to achieve optimal mechanical properties along both axes. Additionally, since fiber architecture is linked to neutrophil inflammation, as these parameters change, a balance must be struck between fiber diameters and alignments that provide better mechanical strength while also preserving the NET-preventing qualities of touch-spun materials. Another limitation of this study is related to its timescale. Aside from the release study, mechanical properties were assessed after 90 minutes of incubation in HBSS at 37 °C. Although the degradation profile of PDO is well documented, to determine how these grafts degrade over time and respond to cyclic loading, long-term studies should be conducted [38, 41]. The templates were also tested without cellular or platelet pre-seeding or pre-clotting. For the purposes and scope of this stage of investigation, this is reasonable, but to further assess the efficacy of these materials, they should be pre-treated and then tested, especially regarding burst pressure. After in vitro evaluation, it would be necessary to determine the mechanical and immunological effects of these templates in vivo; however, this study was a crucial preliminary step towards this end. Another limitation of this study involved the granularity of the concentrations assessed. Now that there is an established benefit to incorporating Manuka honey into touch-spun vascular grafts, and the cytotoxic limit of 10% Manuka honey found in traditionally electrospun templates has been circumvented by this newer fabrication technique, additional concentrations, including those above 10%, should be assessed [22, 24]. Additionally, polymers other than polydioxanone should be assessed, including natural polymers and polymer mixtures, to further optimize the mechanical and biological properties of touch-spun templates. For the purposes of this study, a well-characterized, widely used, clinically approved polymer was employed to minimize variables other than Manuka honey concentration.

Mechanical properties of these grafts were compared to literature values that have been previously cited in vascular tissue engineering, including the Young's modulus of the linear portion of the stress-strain curve. Recently, more emphasis has been placed on the "toe region" of stress-strain curves involving biological materials, especially those containing elastin. Literature values for the toe region Young's modulus are currently very limited, impairing the ability to

compare in a one-for-one way for this investigation. The closest reliable source for a comparable value involved the Young's modulus of dermal skin with varying elastin contents [53]. As such, this investigation calculated the Young's modulus in the toe region for the touch-spun materials and compared it with the modulus previously reported by Zhou et. al. Analysis of the toe region of the stress-strain curves revealed that while the Young's modulus values were statistically significantly higher than the Young's modulus within the toe region of more physiologically relevant materials, they were far more in alignment than ePTFE. It is also of note that the stress-strain curves are much more similar to native tissues in the initial loading stage or toe region than ePTFE grafts, which have a much higher and more linear slope, indicating that the touch-spun materials behave more mechanically like native tissues.

While the results from electron microscopy are promising, they are limited in their ability to definitively quantify neutrophil NETosis, as this has not been extensively characterized at fibrous biomaterial interfaces using SEM. While SEM offers high-resolution visualization of cell–material interactions and extracellular structures, its application to the study of NET formation in this setting remains limited. Consequently, there is a lack of well-established morphological benchmarks against which observed structures can be directly compared, making it challenging to conclusively define NETosis-related features at fibrous interfaces. Variability in biomaterial architecture, fiber diameter, surface chemistry, and imaging preparation further complicates interpretation, as these factors may influence neutrophil adhesion, activation, and the apparent organization of extracellular DNA. Several limitations warrant careful interpretation of NET-related observations. NETs, composed of decondensed chromatin fibers that are inherently delicate and mechanically fragile, are particularly vulnerable to disruption during SEM sample preparation. Processing steps such as fixation, dehydration, drying, and conductive coating can distort, collapse, or fragment these extracellular structures, potentially leading to underrepresentation or mischaracterization of NET architecture. Consequently, NET morphology, continuity, and abundance should be interpreted cautiously. Advances in imaging and preservation techniques may improve the reliability of NET visualization in future studies. As a result, while SEM provides valuable qualitative insight into neutrophil behavior at the biomaterial surface, caution is warranted when assigning definitive NET phenotypes based solely on morphology. Thus, these data provided qualitative images to further corroborate the quantitative MPO ELISA data. Although NET-related analysis remains limited in SEM, it revealed surprising details about neutrophil dynamics at fiber interfaces. Namely, the complete wrapping around of fibers, and in some cases, multiple fibers at a time, as demonstrated by Figure 17, potentially indicating an attempt to engulf. These images depict cellular behaviors in close detail that have not been previously reported, warranting further investigation into neutrophil function and morphology at fibrous biomaterial interfaces.

Additionally, since both Manuka honey and its constitutive component, methyl syringate, have proven effective at reducing neutrophil-mediated inflammation, and the method of touch-spinning has enhanced the efficacy of Manuka honey when incorporated into porous biomaterials, the next phase of research should involve the incorporation of methyl syringate into touch-spun and traditional electrospun biomaterials, and compare their mechanical properties and efficacy at modulating neutrophil inflammatory behaviors. While studies in food science have reported adverse effects on antioxidant activity, total phenolic content, and flavonoid availability, methyl syringate is not a strongly charged molecule and may be more amenable to electrospinning. Since methyl syringate has not yet been used in biomaterial applications, it is important to first characterize its behavior using conventional "gold standard" techniques to minimize unknown variables, and then to use touch-spinning with methyl syringate. These investigations are currently underway and will further elucidate key functional differences between whole Manuka honey and methyl syringate, especially as a biomaterial additive.

Conclusions

Overall, the findings of these investigations pave the way for the viable use of synthetic small-diameter vascular grafts in the operating room, with higher patency rates. By utilizing bioactive therapeutics and fabrication methods that maximize their efficacy to reliably attenuate the neutrophil response to the implant, the cascade leading to continued acute inflammation and, ultimately, device failure can be prevented. This study's aim was to open a new frontier in biomaterial fabrication techniques, design, and incorporation of anti-inflammatory compounds that modulate neutrophil inflammation to promote host tissue regeneration. Future studies will focus on platelet activation, thrombogenicity, and smooth muscle cell seeding onto these biomaterials. Additionally, in vivo large-animal studies are needed to assess systemic inflammation and cytokine levels in response to implantation, template reendothelialization, and end-stage fibrosis at long-term time points.

Availability of Data and Materials

All raw data, statistical analysis codes, and data visualization codes supporting the conclusions of this article will be made available by the authors upon request.

Ethics Approval and Consent to Participate

The study was conducted in accordance with the guidelines of the Declaration of Helsinki and was approved by the Institutional Review Board of the University of Memphis, protocol code #PRO-FY2020-230, dated November 8, 2022. Informed consent was obtained from all subjects involved in the study.

Acknowledgment

The authors thank Dr. Felio Perez for his assistance in scanning electron microscopy and sample preparation, and Dr. Isaac Rodriguez for his mentorship in the mechanical testing.

Funding

This research was funded by the National Institutes of Health, Department of Health and Human Services, National Institute of Biomedical Imaging and Bioengineering, award number 1R15EB033752-01A1.

Conflict of Interest

The authors declare that they have no conflict of interest.

Author Contributions

Evan N. Main: Data curation, formal analysis, investigation, validation, visualization, preparation, conceptualization, methodology, writing – original draft, writing – review and editing; **Alexandra E. Snyder:** Investigation, validation, data curation, writing – review and editing; **Audrey N. Alberson:** Investigation, validation, writing – original draft, writing – review and editing; **Jada K. Sandridge:** Conceptualization, methodology, preparation, writing – review and editing; **Adeline E. Nordmoe:** Investigation, preparation; **Gary L. Bowlin:** Funding acquisition, resources, project administration, supervision, conceptualization, methodology, writing – review and editing.

References

[1] Zoghbi W.A., Duncan T., Antman E., Barbosa M., Champagne B., Chen D., et al. Sustainable development goals and the future of cardiovascular health: a statement from the global cardiovascular disease taskforce. Journal of the American Heart Association. 2014;3:e000504.

[2] Mathers C.D., Loncar D. Projections of global mortality and burden of disease from 2002 to 2030. PLoS medicine. 2006;3:e442.

[3] Antoniou G.A., Chalmers N., Georgiadis G.S., Lazarides M.K., Antoniou S.A., Serracino-Inglott F., et al. A meta-analysis of endovascular versus surgical reconstruction of femoropopliteal arterial disease. Journal of vascular surgery. 2013;57:242-53.

[4] Pashneh-Tala S., MacNeil S., Claeyssens F. The tissue-engineered vascular graft—past, present, and future. Tissue Engineering Part B: Reviews. 2016;22:68-100.

[5] Go A.S., Mozaffarian D., Roger V.L., Benjamin E.J., Berry J.D., Borden W.B., et al. Heart disease and stroke statistics—2013 update: a report from the American Heart Association. circulation. 2013;127:e6-e245.

[6] Harskamp R.E., Lopes R.D., Baisden C.E., De Winter R.J., Alexander J.H. Saphenous vein graft failure after coronary artery bypass surgery: pathophysiology, management, and future directions. Annals of surgery. 2013;257:824-33.

[7] Brewster D.C., Hospital FMG, School HM. Current controversies in the management of aortoiliac occlusive disease. Journal of vascular surgery. 1997;25:365-79.

[8] Chlupáč J., Filova E., Bačáková L. Blood vessel replacement: 50 years of development and tissue engineering paradigms in vascular surgery. Physiological research. 2009;58:S119-S39.

[9] Anderson J.M. Biological responses to materials. Annual review of materials research. 2001;31:81-110.

[10] Anderson J.M., Rodriguez A., Chang D.T. Foreign body reaction to biomaterials. Semin Immunol. 2008;20:86-100.

[11] Ratner B. Vascular Grafts: Technology Success/Technology Failure. BME Frontiers. 2023;4:0003.

[12] Golden M.A., Hanson S.R., Kirkman T.R., Schneider P.A., Clowes A.W. Healing of polytetrafluoroethylene arterial grafts is influenced by graft porosity. Journal of vascular surgery. 1990;11:838-45.

[13] Main E.N., Bowlin G.L. Potential for Manuka honey-inspired therapeutics to improve the host–biomaterial response. MedComm–Biomaterials and Applications. 2022;1:e18.

[14] Selders G.S., Fetz A.E., Radic M.Z., Bowlin G.L. An overview of the role of neutrophils in innate immunity, inflammation and host-biomaterial integration. Regenerative biomaterials. 2017;4:55-68.

[15] Luo H.R., Loison F. Constitutive neutrophil apoptosis: mechanisms and regulation. American journal of hematology. 2008;83:288-95.

[16] Blackwell T.S., Blackwell T.R., Holden E.P., Christman B.W., Christman J.W. In vivo antioxidant treatment suppresses nuclear factor-kappa B activation and neutrophilic lung inflammation. J Immunol. 1996;157:1630-7.

[17] Stoiber W., Obermayer A., Steinbacher P., Krautgartner W.-D. The role of reactive oxygen species (ROS) in the formation of extracellular traps (ETs) in humans. Biomolecules. 2015;5:702-23.

[18] Metzler K.D., Goosmann C., Lubojemska A., Zychlinsky A., Papayannopoulos V. A myeloperoxidase-containing complex regulates neutrophil elastase release and actin dynamics during NETosis. Cell reports. 2014;8:883-96.

[19] Main E.N., Huang J.C., Bowlin G.L. Methyl Syringate: A Primary Driving Factor in Manuka Honeys Ability to Ameliorate Neutrophil Intracellular ROS Activity and NETosis. Frontiers in Bioscience-Landmark. 2024;29:255.

[20] Minden-Birkenmaier B.A., Cherukuri K., Smith R.A., Radic M.Z., Bowlin G.L. Manuka Honey Modulates the Inflammatory Behavior of a dHL-60 Neutrophil Model Under the Cytotoxic Limit. Int J Biomater. 2019.

[21] Minden-Birkenmaier B.A., Meadows M.B., Cherukuri K., Smeltzer M.P., Smith R.A., Radic M.Z., et al. Manuka honey modulates the release profile of a dHL-60 neutrophil model under anti-inflammatory stimulation. Journal of tissue viability. 2020;29:91-9.

[22] Minden-Birkenmaier B.A., Cherukuri K., Smith R.A., Radic M.Z., Bowlin G.L. Manuka honey modulates the inflammatory behavior of a dHL-60 neutrophil model under the cytotoxic limit. International journal of biomaterials. 2019;2019.

[23] Minden-Birkenmaier B., Meadows M., Cherukuri K., Smeltzer M.P., Radic M., Bowlin G., et al. The Effect of Manuka Honey on dHl-60 Cytokine, Chemokine, and Matrix-Degrading Enzyme Release under Inflammatory Conditions. Med One. 2019;4.

[24] Minden-Birkenmaier B.A., Smith R.A., Radic M.Z., van der Merwe M., Bowlin G.L. Manuka Honey Reduces NETosis on an Electrospun Template Within a Therapeutic Window. Polymers. 2020;12:1430.

[25] Menegazzo L., Ciciliot S., Poncina N., Mazzucato M., Persano M., Bonora B., et al. NETosis is induced by high glucose and associated with type 2 diabetes. Acta diabetologica. 2015;52:497-503.

[26] Muhammad A.I., Liao X., Cullen P.J., Liu D., Xiang Q., Wang J., et al. Effects of nonthermal plasma technology on functional food components. Comprehensive Reviews in Food Science and Food Safety. 2018;17:1379-94.

[27] Pankaj S., Misra N., Cullen P. Kinetics of tomato peroxidase inactivation by atmospheric pressure cold plasma based on dielectric barrier discharge. Innovative Food Science & Emerging Technologies. 2013;19:153-7.

[28] Pankaj S.K., Wan Z., Colonna W., Keener K.M. Effect of high voltage atmospheric cold plasma on white grape juice quality. Journal of the Science of Food and Agriculture. 2017;97:4016-21.

[29] Minden-Birkenmaier B.A., Neuhalfen R.M., Janowiak B.E., Sell S.A. Preliminary investigation and characterization of electrospun polycaprolactone and Manuka honey scaffolds for dermal repair. Journal of Engineered Fibers and Fabrics. 2015;10:155892501501000406.

[30] Tokarev A., Asheghali D., Griffiths I.M., Trotsenko O., Gruzd A., Lin X., et al. Touch-and brush-spinning of nanofibers. Advanced Materials. 2015;27:6526-32.

[31] Uribe-Gomez J., Posada-Murcia A., Shukla A., Alkhamis H., Salehi S., Ionov L. Soft Elastic Fibrous Scaffolds for Muscle Tissue Engineering by Touch Spinning. ACS Applied Bio Materials. 2021;4:5585-97.

[32] Sandridge J.K., Main E.N., Tutor O.G., Bowlin G.L. Fabricating synthetic, small-diameter vascular templates via touch-spinning. Journal of the Mechanical Behavior of Biomedical Materials. 2025:107010.

[33] Aubin H., Mas-Moruno C., Iijima M., Schütterle N., Steinbrink M., Assmann A., et al. Customized interface biofunctionalization of decellularized extracellular matrix: toward enhanced endothelialization. Tissue Engineering Part C: Methods. 2016;22:496-508.

[34] Aldenhoff Y.B., van der Veen F.H., ter Woorst J., Habets J., Poole–Warren LA, Koole LH. Performance of a polyurethane vascular prosthesis carrying a dipyridamole (Persantin®) coating on its lumenal surface. Journal of Biomedical Materials Research: An Official Journal of The Society for Biomaterials and The Japanese Society for Biomaterials. 2001;54:224-33.

[35] Lin C.-H., Hsia K., Ma H., Lee H., Lu J.-H.. In vivo performance of decellularized vascular grafts: a review article. International journal of molecular sciences. 2018;19:2101.

[36] Salehi A., Ernez M., Salido G.L., Cattaneo G. Toward "Green" Vessels: Characterization of Microstructure, Mechanics, and Endothelial Cell Interaction on Three Macro-Tubular Plants for Vascular Tissue Engineering Applications. Advanced Materials Technologies. 2025;10:2401129.

[37] Lupon E., Lellouch A.G., Acun A., Andrews A.R., Oganesyan R., Goutard M., et al. Engineering vascularized composite allografts using natural scaffolds: a systematic review. Tissue Engineering Part B: Reviews. 2022;28:677-93.

[38] Goonoo N., Jeetah R., Bhaw-Luximon A., Jhurry D. Polydioxanone-based bio-materials for tissue engineering and drug/gene delivery applications. European Journal of Pharmaceutics and Biopharmaceutics. 2015;97:371-91.

[39] King III W.E., Bowlin G.L. Near-field electrospinning of polydioxanone small diameter vascular graft scaffolds. Journal of the Mechanical Behavior of Biomedical Materials. 2022;130:105207.
[40] Lelkes K.D., Jezbera D., Svoboda R., Podzimek Š., Loskot J., Nalezinková M., et al. A comprehensive study on the degradation process of medical-grade polydioxanone at low pH. Polymer Testing. 2024;138:108536.
[41] Martins J.A., Lach A.A., Morris H.L., Carr A.J., Mouthuy P.-A. Polydioxanone implants: a systematic review on safety and performance in patients. Journal of biomaterials applications. 2020;34:902-16.
[42] Konig G., McAllister T.N., Dusserre N., Garrido S.A., Iyican C., Marini A., et al. Mechanical properties of completely autologous human tissue engineered blood vessels compared to human saphenous vein and mammary artery. Biomaterials. 2009;30:1542-50.
[43] L'Heureux N., Dusserre N., Konig G., Victor B., Keire P., Wight TN, et al. Human tissue-engineered blood vessels for adult arterial revascularization. Nature medicine. 2006;12:361-5.
[44] Stekelenburg M., Rutten M.C., Snoeckx L.H., Baaijens FP. Dynamic straining combined with fibrin gel cell seeding improves strength of tissue-engineered small-diameter vascular grafts. Tissue Engineering Part A. 2009;15:1081-9.
[45] Fetz A.E., Wallace S.E., Bowlin G.L. Electrospun polydioxanone loaded with chloroquine modulates template-induced NET release and inflammatory responses from human neutrophils. Frontiers in Bioengineering and Biotechnology. 2021;9:652055.
[46] Saito Y., Takahashi I., Iwane K., Okubo N., Nishimura M., Matsuzaka M., et al. The influence of blood glucose on neutrophil function in individuals without diabetes. Luminescence. 2013;28:569-73.
[47] Sato J., Takahashi I., Umeda T., Matsuzaka M., Danjyo K., Tsuya R., et al. Effect of alcohol drinking and cigarette smoking on neutrophil functions in adults. Luminescence. 2011;26:557-64.
[48] Fetz A.E., Neeli I., Rodriguez I.A., Radic M.Z., Bowlin G.L. Electrospun Template Architecture and Composition Regulate Neutrophil NETosis In Vitro and In Vivo. Tissue Engineering. 2017;23.
[49] Radic M., Neeli I. Opposition between PKC isoforms regulates histone deimination and neutrophil extracellular chromatin release. Frontiers in Immunology. 2013;4.
[50] Fetz A.E., King W.E., Minden-Birkenmaier B.A., Bowlin G.L. Methods for Quantifying Neutrophil Extracellular Traps on Biomaterials. In: Rasooly A., Baker H., Ossandon M.R., editors. Biomedical Engineering Technologies. Methods in Molecular Biology: Springer Protocols; 2022. p. 727-42.
[51] Bray D., Bagu J., Koegler P. Comparison of hexamethyldisilazane (HMDS), Peldri II, and critical-point drying methods for scanning electron microscopy of biological specimens. Microscopy research and technique. 1993;26:489-95.
[52] Lee J.T.Y., Chow K.L. SEM sample preparation for cells on 3D scaffolds by freeze-drying and HMDS. Scanning. 2012;34:12-25.
[53] Zhou M., González P.J., Van Haasterecht L., Soylu A., Mihailovski M., Van Zuijlen P., et al. Uniaxial mechanical stretch properties correlated with three-dimensional microstructure of human dermal skin. Biomechanics and modeling in mechanobiology. 2024;23:911-25.
[54] Charlton-Ouw K.M., Nosrati N., Miller 3rd C.C., Coogan S.M., Safi H.J., Azizzadeh A. Outcomes of arteriovenous fistulae compared with heparin-bonded and conventional grafts for hemodialysis access. The journal of vascular access. 2012;13:163-7.
[55] Melchiorri A.J., Hibino N., Best C., Yi T., Lee Y., Kraynak C., et al. 3D-printed biodegradable polymeric vascular grafts. Advanced healthcare materials. 2016;5:319-25.
[56] Leal B.B., Wakabayashi N., Oyama K., Kamiya H., Braghirolli D.I., Pranke P. Vascular tissue engineering: Polymers and methodologies for small caliber vascular grafts. Frontiers in Cardiovascular Medicine. 2021;7:592361.
[57] Wystrychowski W., McAllister T.N., Zagalski K., Dusserre N., Cierpka L., L'Heureux N. First human use of an allogeneic tissue-engineered vascular graft for hemodialysis access. Journal of vascular surgery. 2014;60:1353-7.
[58] Fetz A.E., Neeli I., Buddington K.K., Read R.W., Smeltzer M.P., Radic M.Z., et al. Localized delivery of Cl-amidine from electrospun polydioxanone templates to regulate acute neutrophil NETosis: a preliminary evaluation of the PAD4 inhibitor for tissue engineering. Frontiers in pharmacology. 2018;9:289.
[59] Fetz A.E., Neeli I., Rodriguez I.A., Radic M.Z., Bowlin G.L. Electrospun template architecture and composition regulate neutrophil NETosis in vitro and in vivo. Tissue Engineering Part A. 2017;23:1054-63.
[60] Fetz A.E. Electrospun Biomaterial-Induced Neutrophil Extracellular Traps: Characterization and Regulation for Biomaterial-Guided Tissue Regeneration: The University of Memphis; 2021.
[61] Minden-Birkenmaier B.A. Manuka Honey as a Tissue Engineering Bioactive: Effect on Neutrophil Inflammatory Behavior: The University of Memphis; 2020.
[62] Fetz A.E., Fantaziu C.A., Smith R.A., Radic M.Z., Bowlin G.L. Surface area to volume ratio of electrospun polydioxanone templates regulates the adsorption of soluble proteins from human serum. Bioengineering. 2019;6:78.
[63] Zia A.W., Liu R., Wu X. Structural design and mechanical performance of composite vascular grafts. Bio-Design and Manufacturing. 2022;5:757-85.
[64] Greenwald S., Berry C. Improving vascular grafts: the importance of mechanical and haemodynamic properties. The Journal of pathology. 2000;190:292-9.
[65] Hoerstrup S.P., Zünd G., Sodian R., Schnell A.M., Grünenfelder J., Turina M.I. Tissue engineering of small caliber vascular grafts. European journal of cardio-thoracic surgery. 2001;20:164-9.
[66] Snyder Y., Lasley Q., Jana S. Vascular graft with native-like mechanical properties. Materials Letters. 2023;333:133568.
[67] Minden-Birkenmaier B.A., Meadows M.B., Cherukuri K., Smeltzer M.P., Smith R.A., Radic M.Z., et al. The effect of manuka honey on dHL-60 cytokine, chemokine, and matrix-degrading enzyme release under inflammatory conditions. Med one. 2019;4.
[68] Albuquerque M.T., Nagata J., Bottino M.C. Antimicrobial efficacy of triple antibiotic–eluting polymer nanofibers against multispecies biofilm. Journal of endodontics. 2017;43:S51-S6.
[69] Fetz A.E., King III W.E., Minden-Birkenmaier B.A., Bowlin G.L. Methods for Quantifying Neutrophil Extracellular Traps on Biomaterials. Biomedical Engineering Technologies: Volume 2: Springer; 2022. p. 727-42.
[70] Ling S., Xu J.-W. NETosis as a pathogenic factor for heart failure. Oxidative Medicine and Cellular Longevity. 2021;2021.
[71] Sabbatini M., Magnelli V., Renò F. NETosis in wound healing: when enough is enough. Cells. 2021;10:494.
[72] Khan A.A., Alsahli M.A., Rahmani A.H. Myeloperoxidase as an active disease biomarker: recent biochemical and pathological perspectives. Medical sciences. 2018;6:33.
[73] Rizo-Téllez S.A., Sekheri M., Filep J.G. Myeloperoxidase: regulation of neutrophil function and target for therapy. Antioxidants. 2022;11:2302.
[74] Zhang C., Ji R., Yang J. A novel role for leukocyte-derived myeloperoxidase in neointimal hyperplasia after angioplasty. Wiley Online Library; 2006.
[75] Yang J., Cheng Y., Ji R., Zhang C. Novel model of inflammatory neointima formation reveals a potential role of myeloperoxidase in neointimal hyperplasia. American Journal of Physiology-Heart and Circulatory Physiology. 2006;291:H3087-H93.
[76] Snyder A.E., Main E.N., Bowlin G.L. Immunomodulation and Mechanical Characterization of Manuka Honey-Incorporated Near-Field Electrospun Bioresorbable Vascular Grafts. Bioengineering. 2025;12:1270.
[77] Snyder A.E., Sandridge J.K., Nordmoe A.E., Main E.N., Bowlin G.L. Fabrication and mechanical characterization of near field electrospun bioresorbable vascular grafts with fibrous architecture mimicking the arterial extracellular matrix. Journal of Bioactive and Compatible Polymers. 2024;39:455-66.